Mathematical Biosciences and Engineering

https://www.aimspress.com/journal/mbe

MBE, 21(4): 4956–4988.
DOI: 10.3934/mbe.2024219
Received: 18 December 2023
Revised: 09 February 2024
Accepted: 22 February 2024
Published: 01 March 2024

Research article

A deterministic transmission model for analytics-driven optimization of COVID-19 post-pandemic vaccination and quarantine strategies

C. K. Mahadhika and Dipo Aldila*

Department of Mathematics, Faculty of Mathematics and Natural Sciences, Universitas Indonesia, Depok 16424, Indonesia

* **Correspondence:** Email: aldiladipo@sci.ui.ac.id.

Abstract: This study developed a deterministic transmission model for the coronavirus disease of 2019 (COVID-19), considering various factors such as vaccination, awareness, quarantine, and treatment resource limitations for infected individuals in quarantine facilities. The proposed model comprised five compartments: susceptible, vaccinated, quarantined, infected, and recovery. It also considered awareness and limited resources by using a saturated function. Dynamic analyses, including equilibrium points, control reproduction numbers, and bifurcation analyses, were conducted in this research, employing analytics to derive insights. Our results indicated the possibility of an endemic equilibrium even if the reproduction number for control was less than one. Using incidence data from West Java, Indonesia, we estimated our model parameter values to calibrate them with the real situation in the field. Elasticity analysis highlighted the crucial role of contact restrictions in reducing the spread of COVID-19, especially when combined with community awareness. This emphasized the analytics-driven nature of our approach. We transformed our model into an optimal control framework due to budget constraints. Leveraging Pontriagin's maximum principle, we meticulously formulated and solved our optimal control problem using the forward-backward sweep method. Our experiments underscored the pivotal role of vaccination in infection containment. Vaccination effectively reduces the risk of infection among vaccinated individuals, leading to a lower overall infection rate. However, combining vaccination and quarantine measures yields even more promising results than vaccination alone. A second crucial finding emphasized the need for early intervention during outbreaks rather than delayed responses. Early interventions significantly reduce the number of preventable infections, underscoring their importance.

Keywords: deterministic transmission model; post-pandemic strategies; COVID-19; vaccination; public awareness; quarantine; reproduction number; optimal control; analytics assessment

1. Introduction

The coronavirus disease of 2019 (COVID-19) is a disease caused by the severe acute respiratory syndrome coronavirus 2 (SARS-CoV-2) virus and was declared a pandemic by The World Health Organization (WHO) on March 11, 2020 [1]. Symptoms of COVID-19 include fever, cough, shortness of breath, fatigue, headache, nausea, vomiting, sore throat, and diarrhea. These symptoms typically appear about two to 14 days after the infection [2]. As of July 5, 2023, a total of 6,811,818 people in Indonesia have been reported infected with this virus, and 161,867 people have died from the infection [3]. Even though Indonesia has transitioned from the pandemic phase to the endemic phase of COVID-19 [4], it is important to note that the symptoms of COVID-19 can be exacerbated by the presence of comorbidities or underlying health conditions [5], and there are still reported cases of mortality due to COVID-19 [6]. Therefore, it remains crucial to continue practicing preventive measures against COVID-19.

Since the advent of COVID-19, which began affecting various parts of the world in late 2019, numerous scientific approaches have been implemented to comprehend the spread and control of the virus. These approaches encompass medical and public health [7, 8] and social [9, 10], mathematical [11–15], and many other perspectives. In the field of mathematics, the approaches employed by the authors are quite diverse. These range from ordinary differential equations (ODEs) [12–16] to fractional differential equations [11, 17, 18], partial differential equations [19, 20], stochastic models [21, 22], and the utilization of big data analysis approaches [23, 24].

Mathematical modeling is a crucial tool for examining and understanding the dynamics of COVID-19 transmission, particularly in the context of specific interventions. The most popular intervention in the early spread of COVID-19 is the implementation of social distancing. Some authors have introduced their mathematical model to analyze the impact of social distancing on controlling COVID-19. Aldila et al. [25] developed a model to assess the impact of social distancing policies in the city of Jakarta, Indonesia. They found that the intervention can reduce the spread of COVID-19, but the outbreak of COVID-19 will arise soon when social distancing is relaxed. Another model introduced by Gevertz et al. [26] in their paper considers nonsocially distant individuals. They found that implementing relaxation policies at regular intervals could effectively reduce the peak infectious load. However, it is crucial to note that this schedule is highly sensitive to both parameter values and the frequency of the schedule. Recently, Arik et al. [27] used a fractional-order differential equation to analyze the impact of the environment and social distancing on the spread of COVID-19.

Another intervention that many authors considered in their model is the vaccination strategy [11, 13–15]. Saharan and Tee [28] used a simple susceptible-exposed-infectious-recovered (SEIR) model to analyze the effectiveness of a vaccine in controlling the spread of COVID-19 in Malaysia and Thailand. They used the Holt-Winters method to forecast their model dynamics. A fractional-order model was introduced by the authors in [29] to examine the impact of vaccines on the spread of COVID-19. A diffusion framework was used in their model to analyze the spatial spread of COVID-19. They found from their numerical experiments that it is imperative to implement strategic measures to ensure the timely and efficient distribution of vaccines. A mathematical model was introduced by the author in [30] to analyze the optimal allocation of COVID-19 vaccines in the Philippines. Using their model and data from the Philippines, they found that it is crucial to prioritize the primary vaccination series for the pediatric population (aged 5 to 11) within the first three months. Additionally, it is advisable to administer initial booster shots to individuals aged 12 and older during this timeframe. Please see [12, 31–33] for more

examples of the implementation of a mathematical model to assess the impact of vaccines on the spread of COVID-19.

Other models aim to demonstrate the significance of quarantine in suppressing the spread of COVID-19 [34–38]. These models emphasize the complementary role of quarantine, alongside vaccination, in effectively mitigating the transmission of the virus. Authors in [34, 35] have highlighted that while quarantine alone can reduce the spread of COVID-19 in the long-term, it cannot completely eradicate the virus. Nevertheless, the quarantine program can be combined with other initiatives, such as vaccination [36, 37] and interventions to enhance population awareness [38].

Based on this explanation, we can deduce that the long-term elimination of COVID-19 cannot be accomplished solely through vaccination or quarantine programs when executed in isolation from other factors. An essential element that can enhance the effectiveness of both vaccination and quarantine efforts is heightened public awareness. Consequently, certain models attempted to underscore the role of public awareness in the spread of COVID-19 [38–41]. Collectively, these models highlight that an increase in public awareness can effectively control the spread of COVID-19.

Hospital care and capacity play a crucial role in controlling COVID-19. Adequate hospital resources, such as beds, ventilators, medical staff, and equipment, are essential for managing and treating severe cases of COVID-19. Hospitals provide care for individuals with more severe symptoms, and having sufficient capacity is crucial to ensuring that everyone who needs medical attention can receive it promptly. Adequate and timely medical treatment provided in hospitals plays a crucial role in reducing the impact and transmission of diseases, as evidenced in countries such as the USA, Brazil, India [42] and Indonesia [43]. The availability and proper utilization of resources, such as masks and ventilators, also significantly contribute to the recovery of COVID-19 patients [44]. Moreover, several models highlight that hospitalization, when combined with other interventions like vaccination, can positively contribute to COVID-19 recovery [12]. Some models also indicate limited resources in treatment using a saturated function, leading to the conclusion that treatment resources are an important factor in COVID-19 recovery [45–49].

From the above explanation, it can be broadly seen that maximizing the intensity of vaccine administration, implementing quarantine measures, enforcing social restrictions, and improving the quality of hospitals will increase the possibility of eliminating COVID-19 from the community. However, this comes with the consequence of the high cost associated with the required interventions. Therefore, an optimal intervention is needed to minimize the spread of COVID-19 in the population. One approach that can be taken is to tailor COVID-19 interventions based on field needs—in this case, depending on time. One mathematical approach that can be used is to construct the problem as an optimal control problem. The basic idea of this approach is to treat the intervention u as a time-dependent variable $u(t)$. The aim of this implementation is to minimize the number of infected individuals at the lowest possible cost for interventions. Many authors have introduced mathematical models with optimal control for COVID-19 interventions. The authors in [50] developed an optimal control model to analyze the impact of virus protection on the dynamics of COVID-19. The optimal control model for how COVID-19 spread, considering lockdown measures and asymptomatic cases, is discussed in [51]. They found that implementing a lockdown is essential in the early stages of an outbreak. On the other hand, combining vaccination and treatment is effective in controlling and preventing the spread of COVID-19. A more complex model, introduced by the authors in [52], accommodates the low-high-risk population and three types of interventions, namely isolation, detection, and treatment. Their parameter values were

estimated using infection incidence data from Shanghai (March–April 2022). They found that when the budget is limited, implementing isolation and detection is more effective. On the other hand, if the budget is sufficient, implementing treatment alone is more effective compared to other possible scenarios. For more examples of optimal strategies for COVID-19 control, refer to [53, 54].

From the above explanation, we understand that although many references discuss the implementation of vaccination and quarantine as strategies to control COVID-19, there is still a lack of papers that consider the combined impact of population awareness on the effectiveness of these interventions. Therefore, the objective of this paper is to develop a deterministic model that incorporates vaccination and quarantine compartments while also considering the effects of saturation functions that represent awareness and resource limitations. Given that individuals who have contracted COVID-19 develop immunity to the disease for at least six months [55], this paper considers individuals with prior COVID-19 infections to be immune to the disease. An optimal control approach is also considered in our model to assess the optimal scenario for suppressing the spread of COVID-19 with a low cost of intervention through a combination of vaccination and quarantine.

This paper is organized as follows: The first section discusses the state of the art of the research. In Section 2, we encompass the construction of the model, where we delve into the assumptions employed, the differential equation system, and the transmission diagram. We engage in a comprehensive discussion on model analysis, which includes positivity analysis and the parameterization of model parameters in Section 3. In Section 4, we construct the nondimensionalized version of our model to examine the COVID-19-free equilibrium points, the endemic equilibrium, local stability analysis, and bifurcation analysis. Section 5 discusses a series of numerical experiments incorporating elasticity analysis, sensitivity analysis, and autonomous simulation. We define our optimal control model in Section 6. Several numerical experiments for various scenarios are conducted in this section. Lastly, some discussion and conclusions are provided in Section 7.

2. Model construction

Before constructing the model, it is necessary to determine the assumptions or limitations of the model. In this paper, the following assumptions are made: We assume that the total population remains constant, there are no deaths caused by COVID-19, there is no waning immunity, and vaccination does not provide perfect protection against infection for vaccinated individuals. We assume that a vaccinated individual has better protection against contact with other individuals. Furthermore, we include medical interventions to accelerate the recovery rate of infected individuals. The human population is divided into five compartments based on their health status, namely susceptible (S), vaccinated (V), infected (I), quarantined (Q), and recovered (R).

The model construction process is based on the transmission diagram shown in Figure 1. The modeling process is as follows: In our model, we incorporate the intervention of vaccination with a specific rate denoted as u_1. Under this intervention, vaccinated individuals are segregated into a separate class, denoted as V. It is important to note that, based on many reports [12], COVID-19 vaccines do not offer complete protection against infection. Therefore, vaccinated individuals can still potentially contract COVID-19, albeit at a reduced rate, represented by the parameter β_2. This rate is smaller than the infection rate for susceptible individuals in the S class (β_1). In several reports [56–58], it has been found that individuals who have received vaccination tend to exhibit a heightened awareness toward

the spread of COVID-19. This is attributed to their enhanced knowledge of the dangers of COVID-19, whether acquired through media, social interactions, or other means. An increase in the number of COVID-19 infections tends to heighten public awareness of the disease spread. As the number of infected individuals rises, there is often greater media coverage, discussions, and public discourse surrounding the disease. This increased attention can contribute to a heightened awareness among the general population about the importance of preventive measures, the severity of the situation, and the potential risks associated with the disease [59]. Hence, we consider that the probability of infection should be a monotonically decreasing function of I. Hence, the infection term within the vaccinated class is modeled by a saturated function expressed as $\frac{\beta_2 VI}{1+b_1 I}$.

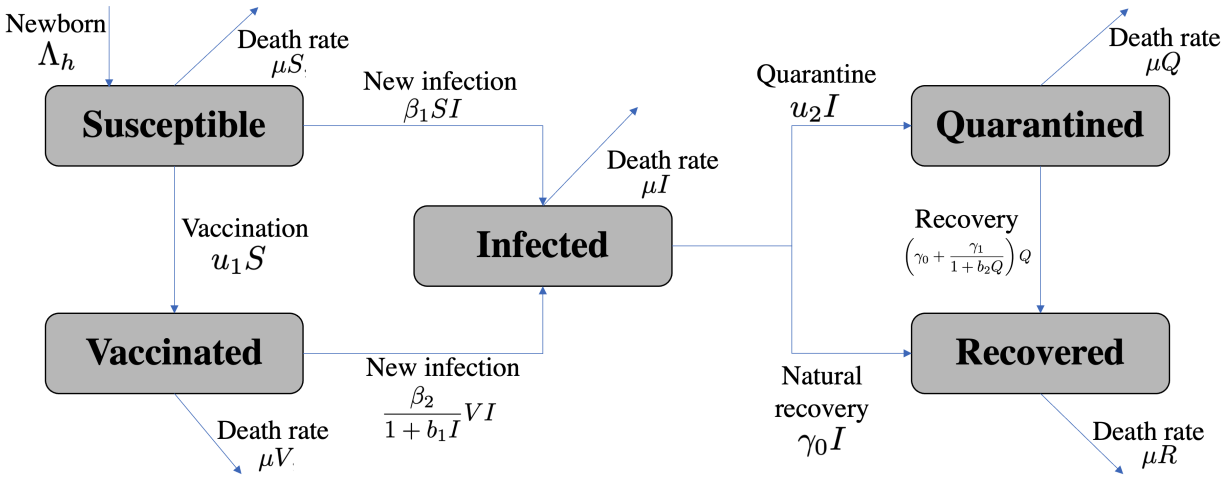

Figure 1. Transmission diagram of compartments.

Additionally, we assume that individuals who become infected can be detected at a rate denoted as u_2. Once detected, individuals receive medical treatment either in a hospital setting or are monitored from home, which we categorize as a quarantine intervention. As a result, their recovery rate increases. Drawing from various reports [60, 61], it has been observed that the escalating number of COVID-19 infection cases during the pandemic may disrupt the quality of hospital services. This phenomenon is attributed, among other factors, such as hospital staff burnout and the presence of resource constraints, as well as challenges in adaptation and mitigation. Public health authorities and healthcare providers frequently collaborate to deploy strategic interventions aimed at effectively managing case surges and mitigating the adverse effects on the standard of healthcare. Based on these facts, we assumed that the recovery rate of quarantined individuals could become saturated due to the high number of individuals in quarantine in the hospital. Therefore, we model the recovery rate of quarantined individuals as a a saturated function $\gamma_0 + \frac{\gamma_1}{1+b_2 Q}$. With this definition of the recovery function, we can see that the recovery rate of quarantined individuals reaches its maximum when Q is relatively small ($Q \approx 0$), i.e., $\gamma_0 + \gamma_1$. On the other hand, when the number of infected individuals is approximately large, the recovery rate for quarantined individuals reaches its minimum level, i.e., γ_0.

Table 1. Table of Parameter in Model (2.1).

Par	Interpretation	Unit	Interval	Ref.	Value	Note
N	Total of human population in West Java	people	4.9×10^7	[62]	4.9×10^6	Assumed
Λ_h	Natural birth rate	$\frac{\text{people}}{\text{day}}$	$[0, \mu N]$	Assumed	$\frac{4\,994\,000}{71.85 \cdot 365}$	Assumed
u_1	Rate of vaccination intervention	$\frac{1}{\text{day}}$	[0,1]	Assumed	0.0344	Estimated
u_2	Rate of quarantine intervention	$\frac{1}{\text{day}}$	[0,1]	Assumed	0.1540	Estimated
β_1	Contact between the susceptible population and the infected population	$\frac{1}{\text{people} \cdot \text{day}}$	$\left[1 \times 10^{-9}, 9.7 \times 10^{-7}\right]$	[63, 64]	$1.4017 \cdot 10^{-7}$	Estimated
μ	Natural death rate	$\frac{1}{\text{day}}$	$\left[\frac{1}{68.79 \times 365}, \frac{1}{77.18 \times 365}\right]$	[65]	$\frac{1}{71.85 \cdot 365}$	Assumed
β_2	Contact between the vaccinated population and the infected population	$\frac{1}{\text{people} \cdot \text{day}}$	$\left[1 \times 10^{-9}, 9.7 \times 10^{-7}\right]$	[63, 64]	$8.4101 \cdot 10^{-8}$	Estimated
γ_0	Natural recovery rate	$\frac{1}{\text{day}}$	$\left[\frac{1}{14}, \frac{1}{7}\right]$	[64, 66]	0.0751	Estimated
γ_1	Maximum additional recovery rate due to quarantine	$\frac{1}{\text{day}}$	$\left[\frac{1}{14}, \frac{1}{7}\right]$	[64, 66]	0.0476	Estimated
b_1	Saturation coefficient due to the number of infected individuals	$\frac{1}{\text{people}}$	$\left[10^{-4}, 0.0179\right]$	[25, 48]	0.0019	Estimated
b_2	Saturation coefficient due to the number of vaccinated individual	$\frac{1}{\text{people}}$	$\left[10^{-4}, 0.0376\right]$	[25, 48]	0.0224	Estimated

Based on the assumptions outlined above, the mathematical model for the spread of COVID-19 is formulated as follows:

$$\frac{dS}{dt} = \Lambda_h - u_1 S - \beta_1 S I - \mu S, \tag{2.1a}$$

$$\frac{dV}{dt} = u_1 S - \frac{\beta_2}{1 + b_1 I} V I - \mu V, \tag{2.1b}$$

$$\frac{dI}{dt} = \beta_1 S I + \frac{\beta_2}{1 + b_1 I} V I - u_2 I - \gamma_0 I - \mu I, \tag{2.1c}$$

$$\frac{dQ}{dt} = u_2 I - \left(\gamma_0 + \frac{\gamma_1}{1 + b_2 Q}\right) Q - \mu Q, \tag{2.1d}$$

$$\frac{dR}{dt} = \gamma_0 I + \left(\gamma_0 + \frac{\gamma_1}{1 + b_2 Q}\right) Q - \mu R, \tag{2.1e}$$

with the parameter description given in Table 1. Since the total population N is $S + V + I + Q + R$, then we have that the dynamic of total population is given by:

$$\frac{dN}{dt} = \Lambda_h - \mu(S + V + I + Q + R) = \Lambda_h - \mu N.$$

If the total of population is approximately constant, then we can approximate the value of Λ_h by assuming $\frac{dN}{dt} = 0$, which lead us to $\Lambda_h = \mu N$.

3. Preliminary analysis

3.1. Positive invariant region

In this section, a nonnegativity analysis of the solution obtained from Model (1) will be performed.

Theorem 1. *Region* Ω *which is defined by:*

$$\Omega = \left\{(S, V, I, Q, R) \in \mathbb{R}^5_+ | 0 < S, V, I, Q, R, S + I + V + Q + R \leq \max\left\{N(0), \frac{\Lambda_h}{\mu}\right\}\right\},$$

is positively invariant with respect to Model (2.1)*.*

Proof. Model (2.1) can be written as follows:

$$\frac{dX}{dt} = CX + D,$$

where:

$$X = [S, V, I, Q, R]^T, \quad D = [\Lambda_h, 0, 0, 0, 0]^T, \quad \text{and} \quad C = \begin{bmatrix} d_1 & 0 & 0 & 0 & 0 \\ u_1 & d_2 & 0 & 0 & 0 \\ \beta_1 I & d_3 & d_4 & 0 & 0 \\ 0 & 0 & u_2 & d_5 & 0 \\ 0 & 0 & \gamma_0 & d_6 & -\mu \end{bmatrix},$$

while $d_1 = -u_1 - \mu - \beta_1 I$, $d_2 = -\frac{\beta_1}{1 + b_1 I} I - \mu$, $d_3 = \frac{\beta_2}{1 + b_1 I} I$, $d_4 = -u_2 - \mu - \gamma_0$, $d_5 = -(\gamma_0 + \frac{\gamma_1}{1 + b_2 Q}) - \mu$, and $d_6 = \gamma_0 + \frac{\gamma_1}{1 + b_2 Q}$. Due to the nonnegative entries outside the main diagonal, matrix C is classified as a Metzler matrix. Since $D \geq 0$, then Model (2.1) possesses a positive invariant in $\mathbb{R}^5_+$ [67]. Hence, all trajectories of solution of Model (2.1), which originate from an initial state in $\mathbb{R}^5_+$, confine forever.

Summing up all equations in Model (2.1), we have:

$$\frac{dN}{dt} = \Lambda_h - \mu N.$$

Then the solution is $N(t) = \frac{\Lambda_h}{\mu} + \left(N(0) - \frac{\Lambda_h}{\mu}\right) e^{\mu t}$. If $N(0) = \frac{\Lambda_h}{\mu}$, then we have $N(t) = \frac{\Lambda_h}{\mu}$ for all time t. If $N(0) < \frac{\Lambda_h}{\mu}$, then $N(t)$ will be monotonically increasing and tends to $\frac{\Lambda_h}{\mu}$ for $t \to \infty$. On the other hand, if $N(0) > \frac{\Lambda_h}{\mu}$, then $N(t)$ will be monotonically decreasing and tends to $\frac{\Lambda_h}{\mu}$ for $t \to \infty$. Therefore, all feasible solutions of the Model (2.1) enter the region Ω, implying that the region is an attracting set.

3.2. Parameter estimation

To estimate the parameters for Model (2.1), a data fitting process was conducted for the number of COVID-19 infections in West Java, Indonesia, from July 1, 2022, to October 1, 2022. In the context of our model, this data represents the dynamics of $I(t)$. Our aim is to fit the dynamic output of $I(t)$ from our model with the available data. Mathematically, this task can be expressed as minimizing the Euclidean distance between COVID-19 incidence data (denoted by I^{data}) and the solution of $I(t)$ from Model (2.1), using the best-fit parameters $\beta_1, \beta_2, u_1, u_2, b_1, b_2, \gamma_0, \gamma_1$, and the best initial conditions $S(0), V(0), I(0), Q(0), R(0)$. Hence, we define the following objective function:

$$C = \int_0^T \left(I^{\text{data}} - I(t)\right)^2 dt, \tag{3.1}$$

where T is the maximum number of existing data points. Our aim is to find the optimal parameters:

$$\Psi^* = \{\beta_1^*, \beta_2^*, u_1^*, u_2^*, b_1^*, b_2^*, \gamma_0^*, \gamma_1^*, S(0)^*, V(0)^*, I(0)^*, Q(0)^*, R(0)^*\},$$

such that:

$$C(\Psi^*) = \min_{\Theta} C(\Psi), \tag{3.2}$$

where Θ is the admissible value for the estimated parameters (fourth column of Table 1). The following constraints need to be mentioned:

- The infection rate of vaccinated individuals (β_2) is smaller than that of susceptible individuals (β_1). Hence, we have $\beta_2 < \beta_1$.
- Vaccination and quarantine is a non-stop intervention by the government. Hence, $u_1 > 0, u_2 > 0$.
- For biological interpretation purposes, we have $\gamma_0, \gamma_1, b_1, b_2$, and all initial conditions are positive.

We approach our parameter estimation challenge as the task of minimizing a constrained, nonlinear, multivariable function. Specifically, our objective is to minimize C subject to the constraints imposed by the ODE model (2.1), while ensuring that the Model parameters and initial conditions adhere to biologically reasonable values. We use the *fmincon* toolbox in MATLAB to solve our problem. The result is shown in Figure 2. The best-fit parameter is provided in Table 1 (sixth column), while the best fit initial condition is as follows:

$$S(0) = 3\,460\,000, V(0) = 1\,870\,000, I(0) = 465, Q(0) = 40, R(0) = 49.$$

For more parameter estimation methods, readers may read [68–71] for further references.

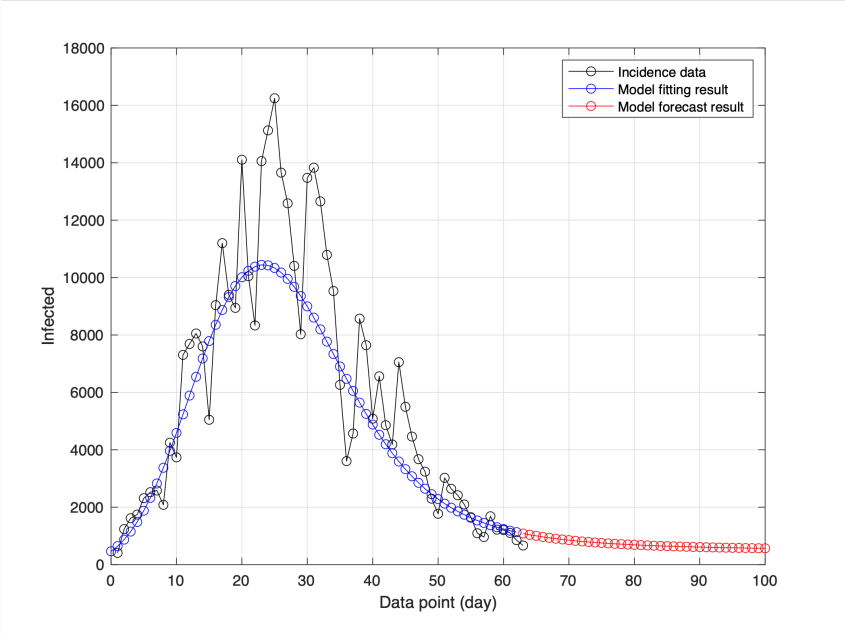

Figure 2. Parameter estimation result using the best-fit parameters. The black dot represents the incidence data (I^{data}), the blue dot represents the model results for compartment I, and the red dot represents the model forecasting result ($I(t)$) until $t = 100$.

From the results of parameter estimation in Table 1, we can see that the control reproduction number is still greater than one, which indicates that the number of infected individuals ($I(t)$) will continue to exist as $t \to \infty$ (see Section 4 for further analytical results on the COVID-19 endemic equilibrium point). We found that $u_1 = 0.0344$ and $u_2 = 0.1540$, which resulted in the findings shown in Figure 2. If the control interventions were stopped ($u_1 = u_2 = 0$), then we would obtain $\mathcal{R}_0 = 9.316$. Any relaxation of the control variables will increase $\mathcal{R}_c$. On the other hand, if we increase the intensity of vaccination and quarantine, then $\mathcal{R}_c$ can be reduced. Figure 3 shows the impact of relaxation/improvement of vaccination and quarantine interventions on the dynamics of infected individuals I.

4. Model analysis

4.1. Nondimensionalization of the model

Let us assume the total population is constant. Hence we have:

$$x_1 = \frac{S}{N}, x_2 = \frac{V}{N}, x_3 = \frac{I}{N}, x_4 = \frac{Q}{N}, x_5 = \frac{R}{N},$$

which represents the proportion of each class to the total human population. Assuming $\tau = t\gamma_0$, $m = \dfrac{\mu}{\gamma_0}, a_1 = \dfrac{\beta_1 N}{\gamma_0}, a_2 = \dfrac{\beta_2}{\gamma_0}, g_1 = \dfrac{\gamma_1}{\gamma_0}, c_1 = \dfrac{b_1}{N}, c_2 = \dfrac{b_2}{N}, e_1 = \dfrac{u_1}{\gamma_0}, e_2 = \dfrac{u_2}{\gamma_0}$, and reducing the susceptible compartments, a nondimensionalized version of the Model (2.1) is obtained as follows:

$$\frac{dx_1}{d\tau} = m - e_1 x_1 - a_1 x_1 x_3 - m x_1,$$

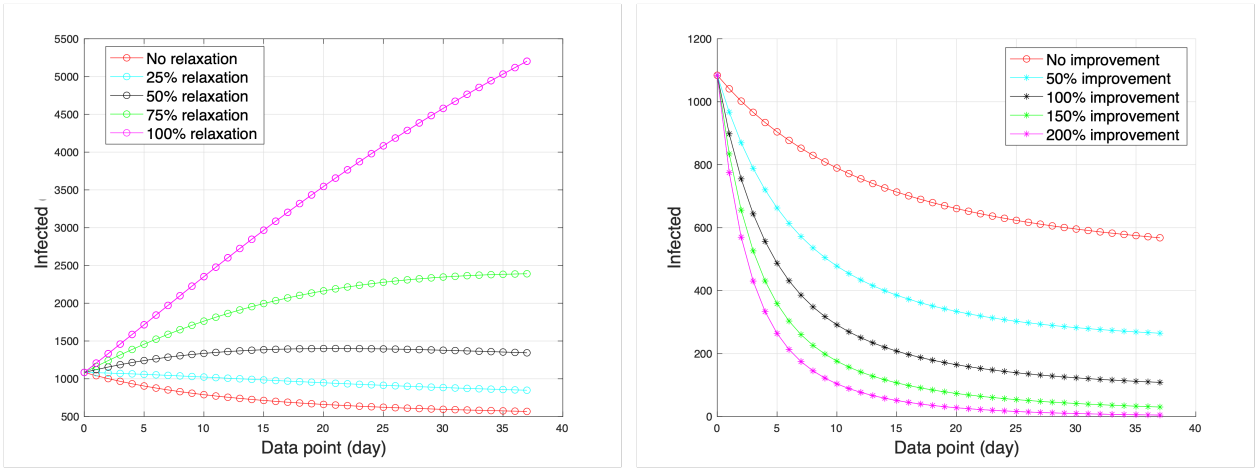

(a) (b)

Figure 3. Forecasting results on the dynamics of infected individuals with vaccination and quarantine interventions, showing (a) relaxed measures and (b) improved measures.

$$\begin{aligned}
\frac{dx_2}{d\tau} &= e_1 x_1 - \frac{a_2}{1 + c_1 x_3} x_2 x_3 - m x_3, \\
\frac{dx_3}{d\tau} &= a_1 x_1 x_3 + \frac{a_2}{1 + c_1 x_3} x_2 x_3 - e_2 x_3 - x_3 - m x_3, \\
\frac{dx_4}{d\tau} &= e_2 x_3 - (1 + \frac{g_1}{1 + c_2 x_4}) x_4 - m x_4,
\end{aligned} \tag{4.1}$$

where $x_5 = 1 - x_1 - x_2 - x_3 - x_4$.

4.2. COVID-19-free equilibrium and the control reproduction number

In this section, we initiate our analysis by determining the form of the COVID-19-free equilibrium, followed by the calculation of the control reproduction number, denoted as $\mathcal{R}_c$. Reproduction numbers have been utilized by various authors in epidemiological models [11,49] to assess the dynamic behavior of the proposed model, including the existence and stability of equilibrium points.

Theorem 2. *The COVID-19-free equilibrium of system* (4.1) *is given by:*

$$\mathcal{E}_0 = (x_1^\dagger, x_2^\dagger, x_3^\dagger, x_4^\dagger) = \left(\frac{m}{m + e_1}, \frac{e_1}{m + e_1}, 0, 0 \right),$$

which always exists unconditionally.

Proof. The equilibrium points associated with Model (1) are obtained when the population changes in each compartment remain constant, namely, when $\frac{dx_1}{d\tau} = 0$, $\frac{dx_2}{d\tau} = 0$, $\frac{dx_3}{d\tau} = 0$, and $\frac{dx_4}{d\tau} = 0$. As the COVID-19-free equilibrium point represents a condition without COVID-19 in the population, we have $x_3^\dagger = 0$. By direct calculation, substituting $x_3^\dagger = 0$ into $\frac{dx_1}{dt}$, $\frac{dx_2}{dt}$, and $\frac{dx_4}{dt}$, we obtain $x_1^\dagger = \frac{m}{m + e_1}$, $x_2^\dagger = \frac{e_1}{m + e_1}$, and $x_4^\dagger = 0$. From the expressions of $x_1^\dagger$, $x_2^\dagger$, $x_3^\dagger$, and $x_4^\dagger$, it is clear that they always exist in $\mathbb{R}^4_{\geq 0}$ without any existence criteria. Hence, the proof is complete.

From the direct consequences of the expression of $\mathcal{E}_0$, we have the following corollary.

Corollary 1. *Without the intervention of vaccination, the COVID-19-free equilibrium of system* (4.1) *is given by:*

$$\mathcal{E}_0^* = (x_1^\dagger, x_2^\dagger, x_3^\dagger, x_4^\dagger) = (1, 0, 0, 0).$$

Theorem 3. *The control reproduction number from system* (4.1) *is* $\mathcal{R}_c = \dfrac{a_1 m + a_2 e_1}{(e_2 + 1 + m)(m + e_1)}$.

Proof. We use a next-generation matrix approach [72] to determine the control reproduction number of the system (4.1). At first, we determine the Jacobian matrix of the subsystem of (4.1) that only involves the infected compartments x_3 and x_4. The Jacobian matrix evaluated at $\mathcal{E}_0$ is given by:

$$J = \begin{bmatrix} \dfrac{a_1 m}{m + e_1} + \dfrac{a_2 e_1}{(m + e_1)} - e_2 - 1 - m & 0 \\ e_2 & -1 - g_1 - m \end{bmatrix}. \tag{4.2}$$

The matrix J can be written as the sum of the transmission matrix T and the transition matrix Σ, where:

$$T = \begin{bmatrix} \dfrac{a_1 m}{m + e_1} + \dfrac{a_2 e_1}{(m + e_1)} & 0 \\ 0 & 0 \end{bmatrix} \quad \text{and} \quad \Sigma = \begin{bmatrix} -1 - m - e_2 & 0 \\ e_2 & -1 - g_1 - m \end{bmatrix}.$$

Since the second row of matrix T consists entirely of zeros, the next-generation matrix can be derived as:

$$NGM = -\mathbf{E}'\mathbf{T}\boldsymbol{\Sigma}^{-1}\mathbf{E} = \left[\frac{a_1 m + a_2 e_1}{(e_2 + 1 + m)(m + e_1)}\right],$$

where $\mathbf{E} = \begin{bmatrix} 1 \\ 0 \end{bmatrix}$ and $\mathbf{E}'$ is the transpose of $\mathbf{E}$. Since the spectral radius of the matrix above is given by $\dfrac{a_1 m + a_2 e_1}{(e_2 + 1 + m)(m + e_1)}$, we can conclude that $\mathcal{R}_c = \dfrac{a_1 m + a_2 e_1}{(e_2 + 1 + m)(m + e_1)}$. Hence, the proof is complete.

4.3. The existence of COVID-19 endemic equilibrium point

Theorem 4. *Let* $\mathcal{R}_c^*$ *be* $\mathcal{R}_c$ *that satisfies* $k_1^2 - 4k_0k_2 = 0$ *and* $\mathcal{K} = (e_2 + 1 + m)^2(m + e_1) - a_2e_1(e_2 + 1 + m) + a_2e_1(mc_1 + a_2)$*, then, system* (4.1) *has:*

1) One endemic equilibrium if $\mathcal{R}_c > 1$*,*
2) No endemic equilibrium for $\mathcal{R}_c < 1$ *if* $\mathcal{K} \geq 0$*,*
3) No endemic equilibrium for $\mathcal{R}_c < \mathcal{R}_c^* < 1$ *if* $\mathcal{K} < 0$*,*
4) Two endemic equilibrium for $\mathcal{R}_c^* \leq \mathcal{R}_c < 1$ *if* $\mathcal{K} < 0$*.*

Proof. The endemic equilibrium represents a condition in which the disease persists within the system [73], specifically at the point (x_1, x_2, x_3, x_4) with $x_3 \neq 0$. As there is no change in the system when the endemic equilibrium point is reached, we set $\dfrac{dx_1}{d\tau} = 0$, $\dfrac{dx_2}{d\tau} = 0$, $\dfrac{dx_3}{d\tau} = 0$, and $\dfrac{dx_4}{d\tau} = 0$ with $x_3 \neq 0$. By direct calculation, we can find:

$$\mathcal{E}_1 = (x_1^*, x_2^*, x_3^*, x_4^*), \tag{4.3}$$

where $x_1^* = \dfrac{m}{a_1 x_3^* + m + e_1}$, $x_2^* = \dfrac{e_1 m\left(c_1 x_3^* + 1\right)}{\left(a_1 x_3^* + m + e_1\right)\left(m c_1 x_3^* + m + a_2 x_3^*\right)}$, x_4^* is the positive root of $e_2 x_3^* - \left(1 + \dfrac{g_1}{c_1 x_4^* + 1}\right) x_4^* - m x_4^* = 0$, and x_3* is taken from the positive roots of the following polynomial:

$$f(x_3^*) = k_2 x_3^{*2} + k_1 x_3^* + k_0 = 0, \tag{4.4}$$

where:

$$\begin{aligned} k_2 &= -\frac{(e_2 + 1 + m)(m c_1 + a_2)\left(\mathcal{R}_c (e_2 + 1 + m)(m + e_1) - a_2 e_1\right)}{m}, \\ k_1 &= ((e_2 + 1 + m)(c_1(\mathcal{R}_c - 1)m^2 - \mathcal{R}_c(e_2 + 1 + m)^2(m + e_1) \ldots \\ &\quad + (c_1 e_1 + a_2)(\mathcal{R}_c - 1)m + \mathcal{R}_c a_2 e_1) - a_2 e_1(m c_1 + a_2)), \\ k_0 &= m(e_2 + 1 + m)(m + e_1)(\mathcal{R}_c - 1). \end{aligned}$$

To analyze the existence of the endemic equilibrium, it is necessary to guarantee the existence of a positive root in the polynomial (4.4). If the roots are positive, then x_1^*, x_2^*, and x_4^* will also be positive. From Descartes' rule of signs, it can be concluded that when $\mathcal{R}_c > 1$, the system will have a unique endemic equilibrium point. Furthermore, for $k_0 < 0$, it is possible for the system to have zero or two positive roots. Hence, further analysis is needed. Gradient analysis is conducted at $\mathcal{R}_c = 1, x_3 = 0$. Using implicit derivative on polynomial (4.4), we have:

$$\frac{\partial f(x_3)}{\partial \mathcal{R}_c}\Big|_{\mathcal{R}_c = 1, x_3 = 0} = \frac{m(e_2 + 1 + m)(m + e_1)}{(e_2 + 1 + m)^2(m + e_1) - (e_2 + 1 + m) a_2 e_1 + [a_2 e_1 (m c_1 + a_2)]}. \tag{4.5}$$

Table 2. The maximum number of roots for x_3^* can be determined using Descartes' rule of signs for the equation in (4.4).

Case	k_2	k_1	k_0	$\mathcal{R}_c$	Change of Sign	Number of Possible Roots
1	-	+	-	$\mathcal{R}_c < 1$	0	0 or 2
2	-	+	+	$\mathcal{R}_c > 1$	1	1
3	-	-	-	$\mathcal{R}_c < 1$	2	0
4	-	-	+	$\mathcal{R}_c > 1$	1	1

Hence, if $\mathcal{K} = (e_2 + 1 + m)^2(m + e_1) - (e_2 + 1 + m) a_2 e_1 + [a_2 e_1 (m c_1 + a_2)] < 0$, then we will have a negative gradient of x_3 at $\mathscr{R}_c = 1, x_3 = 0$. This indicates the existence of positive roots x_3 for some intervals when $\mathcal{R}_c < 1$. Since $f(x_3^*)$ is a second-degree polynomial, then $f(x_3^*)$ will have a turning point at $\mathcal{R}_c = \mathcal{R}_c^*$, where $\mathcal{R}_c^*$ is the value of $\mathcal{R}_c$ that satisfies the discriminant of $f(x_3^*)$ equal to zero, which is $k_1^2 - 4k_0k_2 = 0$. Hence, we have proved case 3 of the theorem. If $\mathcal{R}_c < \mathcal{R}_c^*$, then we will have no positive root (case 4 of the theorem proved). Lastly, if $\mathcal{K} \geq 0$, then we will have a positive gradient, which confirms case 2 in the proven theorem. Furthermore, we use Descartes' rule of signs to determine the possible number of positive roots of the polynomial $f(x_3)$. The results are shown in Table 2. It can be observed that $f(x_3)$ may have 0, 1, or 2 positive roots. Additionally, it is possible to have an endemic equilibrium even when $\mathcal{R}_0 < 1$.

4.4. Local stability analysis

In the previous section, we have shown that the COVID-19-free equilibrium always exists, while the endemic equilibrium exists depending on the conditions of $\mathcal{R}_c$ and $\mathcal{K}$. In this section, we show how the stability of the COVID-19-free equilibrium can only be achieved if $\mathcal{R}_c < 1$.

Theorem 5. *For $e_1 \neq 0$ and $e_2 \neq 0$, the point $\mathcal{E}_0$ in the system (1) is locally asymptotically stable if $\mathcal{R}_c < 1$ and unstable if $\mathcal{R}_c > 1$.*

Proof. To demonstrate the stability of the COVID-19-free equilibrium point, we linearize system (4.1) around the COVID-19-free equilibrium point [73]. The Jacobian matrix is formulated as follows:

$$Jac_{|DFE} = \begin{bmatrix} -m - e_1 & 0 & -\dfrac{a_1 m}{m + e_1} & 0 \\ e_1 & -m & -\dfrac{a_2 e_1}{(m + e_1)} & 0 \\ 0 & 0 & \dfrac{a_1 m}{m + e_1} - 1 + \dfrac{a_2 e_1}{(m + e_1)} - e_2 - m & 0 \\ 0 & 0 & e_2 & (-m - 1) - g_1 \end{bmatrix}. \tag{4.6}$$

The eigenvalues of the matrix above can be obtained as follows:

$$\begin{aligned} \lambda_1 &= -m, \\ \lambda_2 &= -(m + e_1), \\ \lambda_3 &= -(m + 1 + g_1), \\ \lambda_4 &= -\frac{m^2 - m a_1 + m e_1 + m e_2 + e_1 e_2 + m + e_1 - a_2 e_1}{(m + e_1)}, \\ &= (\mathcal{R}_c - 1)(e_2 + 1 + m). \end{aligned}$$

$\mathcal{E}_0$ is locally asymptotically stable if all eigenvalues of matrix (4.6) have negative values. Since λ_1 to λ_3 are already negative and $\lambda_4 < 0$ for $\mathcal{R}_c < 1$, $\mathcal{E}_0$ is locally asymptotically stable for $\mathcal{R}_c < 1$. Moreover, $\mathcal{E}_0$ is unstable if any eigenvalue of matrix (4.6) is positive. Therefore, $\mathcal{E}_0$ is unstable for $\mathcal{R}_c > 1$.

4.5. Bifurcation analysis

Here, we analyze the local stability of the COVID-19 endemic equilibrium point near the condition $\mathcal{R}_c = 1$ using the Castillo-Song bifurcation theorem [74].

Theorem 6. *The COVID-19 model in system* (4.1) *undergoes backward bifurcation at $\mathcal{R}_c = 1$ if $\mathcal{K} < 0$, and forward bifurcation when $\mathcal{K} > 0$.*

Proof. Using the Castillo-Song theorem [74], we examine bifurcation from system (2.1), which has already been nondimensionalized to become system (4.1). System (4.1) can be represented as follows:

$$\begin{aligned} f_1 &= m - e_1 x_1 - a_1 x_1 x_3 - m x_1, \\ f_2 &= e_1 x_1 - \frac{a_2}{1 + c_1 x_3} x_2 x_3 - m x_3, \\ f_3 &= a_1 x_1 x_3 + \frac{a_2}{1 + c_1 x_3} x_2 x_3 - e_2 x_3 - x_3 - m x_3, \end{aligned}$$

$$f_4 = e_2 x_3 - (1 + \frac{g_1}{1 + c_2 x_4}) x_4 - m x_4.$$

For $\mathcal{R}_c = 1$, we take the bifurcation parameter $a_1 = a_1^*$ where a_1 represents the contact rate β_1. We have:

$$a_1^* = \frac{(e_2 + 1 + m)(m + e_1) - a_2 e_1}{m}.$$

Furthermore, the linearization matrix around the COVID-19-free equilibrium point for $a_1 = a_1^*$ is obtained as follows:

$$J = \begin{bmatrix} -m - e_1 & 0 & \frac{-(e_2 + 1 + m)(m + e_1) + a_2 e_1}{(m + e_1)} & 0 \\ e_1 & -m & -\frac{a_2 e_1}{(m + e_1)} & 0 \\ 0 & 0 & 0 & 0 \\ 0 & 0 & e_2 & (-m - 1) - g_1 \end{bmatrix}.$$

Subsequently, we computed the right and left eigenvectors of the zero eigenvalues of $\mathcal{A}$, denoted as $\mathbf{w} = (w_1, w_2, w_3, w_4)^T$ and $\mathbf{v} = (v_1, v_2, v_3, v_4)$, respectively, yielding the following expression:

$$\begin{aligned} w_1 &= -\frac{((m + 1) + g_1)((e_2 + 1 + m)(m + e_1) - a_2 e_1)}{e_2 (m + e_1)^2}, \\ w_2 &= -\frac{((e_2 + 1 + m)(m + e_1) + m a_2)((m + 1) + g_1) e_1}{e_2 (m + e_1)^2 m}, \\ w_3 &= \frac{m + 1 + g_1}{e_2}, \quad w_4 = w_4, \\ v_1 &= 0, \quad v_2 = 0, \quad v_3 = v_3, \quad v_4 = 0. \end{aligned}$$

Using the theorem [74] and computing the nonzero partial derivatives of $f(x)$ at the disease-free equilibrium, the associated bifurcation coefficients are defined as follows:

$$\begin{aligned} \mathcal{A} &= \sum_{\mathrm{k,i,j=1}}^{4} v_k w_i w_j \frac{\partial^2 f_k}{\partial x_i \partial x_j}(0,0), \\ &= -\frac{2\left((e_2 + 1 + m)^2 (m + e_1) - a_2 e_1 (e_2 + 1 + m) + a_2 e_1 (m c_1 + a_2)\right)((m + 1) + g_1)^2}{(m + e_1) m e_2^2}, \\ &= -\frac{2\mathcal{K}((m + 1) + g_1)^2}{(m + e_1) m e_2^2}, \end{aligned} \tag{4.7}$$

$$\begin{aligned} \mathcal{B} &= \sum_{\mathrm{k,i=1}}^{4} v_k w_i \frac{\partial^2 f_k}{\partial x_i \partial {a_1}^*}(0,0), \\ &= \frac{m(m + 1 + g_1)}{(m + e_1) e_2}. \end{aligned} \tag{4.8}$$

Since $\mathcal{B} > 0$, according to [74], backward bifurcation occurs when $\mathcal{A} > 0 \iff \mathcal{K} < 0$, and forward bifurcation occurs when $\mathcal{A} < 0 \iff \mathcal{K} > 0$. Hence, the theorem is proved.

5. Numerical experiments

In this section, we present the results of numerical experiments conducted on model (2.1) regarding the elasticity analysis, bifurcation diagram, and autonomous simulations. The control reproduction number of the original Model in (2.1) is given by:

$$\mathscr{R}_c = \frac{\Lambda\ (\mu\beta_1 + \beta_2 u_1)}{(\mu + u_1)\,\mu\ (u_2 + \gamma_0 + \mu)}.$$

Hence, without any intervention, the basic reproduction number of the original model in (2.1) is given by:

$$\mathscr{R}_0 = \frac{\Lambda\beta_1}{\mu(\mu + \gamma_0)}.$$

All model parameters that have been used in this section are given in Table 1, which shows that $\mathcal{R}_c = 1.827 > 1$. Without any improvement in the control variables, COVID-19 will continue to exist in West Java.

5.1. Elasticity analysis

At this stage, an analysis will be carried out to examine the sensitivity of the control reproduction number ($\mathcal{R}_c$) to various parameters that affect its value, as well as the relationship between these parameters. By considering different values for these parameters, we can observe how the control reproduction number of the system (2.1) varies while keeping the values of the other parameters constant. To evaluate the sensitivity, we employ the forward sensitivity index of $\mathscr{R}_c$, which is denoted by:

$$\mathcal{E}^{\sigma}_{\mathscr{R}_c} = \frac{\partial \mathscr{R}_c}{\partial \sigma} \times \frac{\sigma}{\mathscr{R}_c}, \tag{5.1}$$

where σ is a parameter in the system (2.1).

We calculate the elasticity indices of $\mathscr{R}_c$ with respect to all parameter values to observe the effects of changes in parameters on $\mathscr{R}_c$. Using the formula and parameter values in Table 1, we obtained the following results:

$$\mathcal{E}^{\mu}_{\mathscr{R}_c} = \frac{-2\,\mu^3\beta_1 - ((\beta_1 + 3\,\beta_2)\,u_1 + \beta_1\,(u_2 + \gamma_0))\,\mu^2 - 2\,u_1\beta_2\,(u_1 + u_2 + \gamma_0)\,\mu - {u_1}^2\beta_2\,(u_2 + \gamma_0)}{(\mu\beta_1 + \beta_2 u_1)\,(\mu + u_1)\,(u_2 + \gamma_0 + \mu)} = -0.99,$$

$$\mathcal{E}^{\beta_1}_{\mathscr{R}_c} = \frac{\mu\beta_1}{\mu\beta_1 + \beta_2 u_1} = 0.0018, \quad \mathcal{E}^{\beta_2}_{\mathscr{R}_c} = \frac{\beta_2 u_1}{\mu\beta_1 + \beta_2 u_1} = 0.998, \quad \mathcal{E}^{u_2}_{\mathscr{R}_c} = -\frac{u_2}{u_2 + \gamma_0 + \mu} = -0.673,$$

$$\mathcal{E}^{\gamma_0}_{\mathscr{R}_c} = \frac{\gamma_0}{u_2 + \gamma_0 + \mu} = -0.326, \quad \mathcal{E}^{\gamma_1}_{\mathscr{R}_c} = 0, \quad \mathcal{E}^{u_1}_{\mathscr{R}_c} = -\frac{u_1\,(\beta_1 - \beta_2)\,\mu}{(\mu\beta_1 + \beta_2 u_1)\,(\mu + u_1)} = -0.00073,$$

$$\mathcal{E}^{b_1}_{\mathscr{R}_c} = 0, \quad \mathcal{E}^{b_2}_{\mathscr{R}_c} = 0.$$

To analyze the impact of changes in vaccination intensity and quarantine measures, we recalculate the elasticity index by adjusting the values of u_1 and u_2. The parameters used are the same as those shown in Figure 3. It is evident that reducing the intensity of vaccination and quarantine increases the elasticity of vaccine intervention while decreasing the elasticity of quarantine. Conversely, when we increase the

intensity of vaccination and quarantine, the effectiveness of vaccination decreases while the elasticity of quarantine increases. Additionally, we observe that the quarantine intervention is more elastic in affecting $\mathcal{R}_0$ compared to vaccination. Another noteworthy point from Table 3 is that the infection rate of vaccinated individuals is much more sensitive compared to that of non-vaccinated individuals. Hence, it is essential to develop a high-quality vaccine that can provide maximum protection against the COVID-19 infection.

Table 3. Changes of elasticity index of $\mathcal{R}_c$ with respect to $u_1, u_2, \gamma_0, \beta_1$, and β_2 when u_1 and u_2 are relaxed (reduced) and when it is improved (increased).

Parameter	u_1 and u_2 relaxed				u_1 and u_2 improved			
	25%	50%	75%	85%	50%	100%	150%	200%
u_1	-0.0007	-0.0015	-0.003	-0.004	-0.00049	-0.00036	-0.00029	-0.00024
u_2	-0.607	-0.507	-0.34	-0.236	-0.755	-0.804	-0.837	-0.861
γ_0	-0.392	-0.492	-0.659	-0.763	-0.244	-0.195	-0.162	-0.139
β_1	0.0024	0.0036	0.007	0.012	0.001	0.00092	0.00073	0.0006
β_2	0.997	0.996	0.992	0.987	0.998	0.999	0.999	0.999

5.2. *Bifurcation diagram and autonomous simulation*

In this section, we draw the bifurcation diagram using the best-fit parameter values obtained from the previous section. The result is presented in Figure 4, where the forward bifurcation occurs at $\mathcal{R}_c = 1$. The blue and red curves represent the equilibrium states of COVID-19-free and endemic conditions, respectively. The solid and dotted curves represent the stable and unstable equilibrium points. *BP* denotes the branching point at $\mathcal{R}_c = 1$. It is clear to see that when $\mathcal{R}_c < 1$, the COVID-19-free equilibrium is stable, but it becomes unstable when it surpasses the branching point *BP*. At the same time, at the branching point *BP*, the endemic equilibrium starts to emerge as $\mathcal{R}_c$ increases.

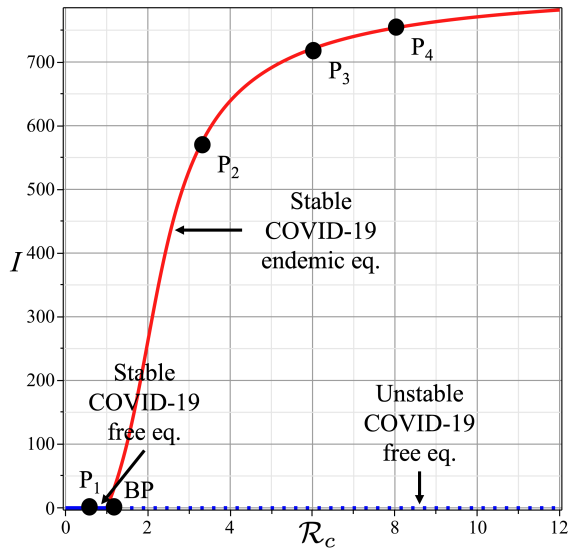

Figure 4. Forward bifurcation of system (4.1). P_i for $i = 1, 2, 3, 4$ is the sample point of $\mathcal{R}_c$ at 0.5, 3.7, 6 and 8, respectively. BP is the branching point at $\mathcal{R}_c = 1$.

To illustrate the dynamics of the Model (2.1), we use four sample points in Figure 4, denoted as P_1, P_2, P_3 and P_4. We observe that P_1 lies in the region where $\mathscr{R}_c < 1$, and the autonomous simulation is shown in Figure 5, panel (a), for the original model in the Model (2.1). It is evident that the system tends toward a stable COVID-19-free equilibrium. On the other hand, for sample points P_2, P_3 and P_4, when $\mathscr{R}_c > 1$, the system tends toward an endemic equilibrium. The numerical simulation results are given in panels (b)–(d), respectively.

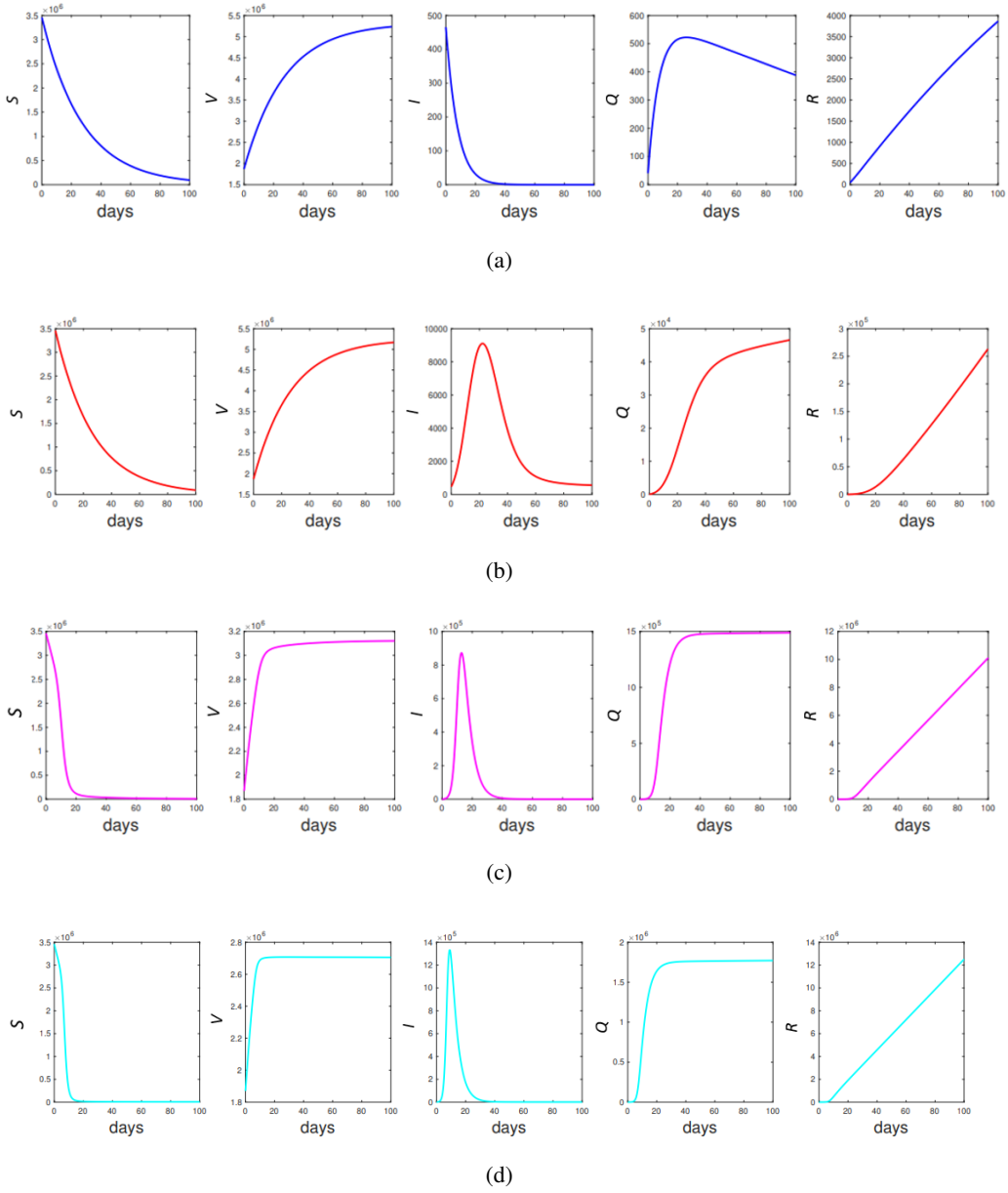

Figure 5. The impact of $\mathscr{R}_c(\beta_1, \beta_2)$ on the dynamics of each compartment from Model (2.1). Panels (a)–(d) represent the sample points P_1 to P_4, as shown in Figure 4. Specific parameter values used in the simulation are given in Table 4.

Table 4. Numerical results on the stable equilibrium points of Model (2.1) depend on $\mathscr{R}_c$.

Point	β_1	β_2	$\mathscr{R}_c$	S	V	I	Q	R
P_1	2.79×10^{-8}	1.11×10^{-8}	0.5	5197	4.98×10^6	0	0	0
P_2	1.4×10^{-7}	8.4×10^{-8}	3.76	5194	3.76×10^6	203	391	1.22×10^6
P_3	6.87×10^{-7}	2.75×10^{-7}	6	5144	1.67×10^6	550	1101	3.3×10^6
P_4	9.16×10^{-7}	3.66×10^{-7}	8	5119	1.32×10^6	610	1223	3.6×10^6

6. Optimal control model

6.1. Optimal control characterization

Model (2.1) considers two control variables: u_1, representing vaccination intervention, and u_2, representing quarantine intervention. Trivially, from our sensitivity analysis in the previous section, we understand that larger values of u_1 and u_2 will yield better results for eradicating COVID-19. However, it will come at a high cost. Hence, our main objective is to minimize the number of infected individuals, I and Q, with the lowest possible cost of u_1 and u_2. To address this problem, we constructed a cost function as follows:

$$J = \int_0^T \left(\omega_1 I + \omega_2 Q + \varphi_1 u_1^2 + \varphi_2 u_2^2\right) dt, \tag{6.1}$$

which represents the total cost due to the high number of infected individuals and the level of control intensity. Note that ω_1 and ω_2 represent the weight parameters for I and Q, respectively. On the other hand, φ_1 and φ_2 represent the weight costs for u_1 and u_2. Next, by applying Pontryagin's maximum principle [75], we obtain the Hamiltonian function as follows:

$$H = \omega_1 I + \omega_2 Q + \varphi_1 u_1^2 + \varphi_2 u_2^2 + \lambda_1 \frac{dS}{dt} + \lambda_2 \frac{dV}{dt} + \lambda_3 \frac{dI}{dt} + \lambda_4 \frac{dQ}{dt} + \lambda_5 \frac{dR}{dt}, \tag{6.2}$$

where λ_1 for $i = 1, 2, 3, 4, 5$ represents the adjoint variables for S, V, I, Q, and R, respectively. Thus, taking the partial derivatives of H with respect to each of the state variables yields the adjoint system, as shown below:

$$\begin{aligned}
\frac{d\lambda_1}{dt} &= -\frac{\partial H}{\partial S} = -\beta_1 I\,\lambda_3 - (-\beta_1 I - \mu - u_1)\,\lambda_1 - u_1\lambda_2, \\
&= \beta_1 I(\lambda_2 - \lambda_3) + u_1(\lambda_1 - \lambda_2) + \mu\lambda_1, \\
\frac{d\lambda_2}{dt} &= -\frac{\partial H}{\partial V} = -\frac{\beta_2 I n\,\lambda_3}{I\,b_1 + 1} - \left(-\frac{\beta_2 I n}{I\,b_1 + 1} - \mu\right)\lambda_2, \\
&= \frac{\beta_2 I}{1 + b_1 I}(\lambda_2 - \lambda_3) + \mu\lambda_2, \\
\frac{d\lambda_3}{dt} &= -\frac{\partial H}{\partial I} = -\omega_1 - \left(\beta_1 S - \frac{\beta_2 V I\,b_1}{(I\,b_1 + 1)^2} + \frac{\beta_2 V}{I\,b_1 + 1} - u_2 - \gamma_0 - \mu\right)\lambda_3 \ldots \\
&\quad -u_2\lambda_4 - \lambda_5\gamma_0 + \beta_1 S\,\lambda_1 - \left(\frac{\beta_2 V I\,b_1}{(I\,b_1 + 1)^2} - \frac{\beta_2 V}{I\,b_1 + 1}\right)\lambda_2, \\
&= -\omega_1 + \beta_1 S(\lambda_1 - \lambda_3) + \frac{\beta_2 V}{1 + b_1 I}\left(1 - \frac{b_1 I}{1 + b_1 I}\right)(\lambda_2 - \lambda_3) + \ldots
\end{aligned} \tag{6.3}$$

$$
\begin{aligned}
& +u_2(\lambda_3-\lambda_4)+\gamma_0(\lambda_3-\lambda_5)+\mu\lambda_3,\\
\frac{d\lambda_4}{dt} &= -\frac{\partial H}{\partial Q} = -\omega_2-\left(\frac{\gamma_1 b_2 Q}{(b_2Q+1)^2}-\gamma_0-\frac{\gamma_1}{b_2Q+1}-\mu\right)\lambda_4-\left(-\frac{\gamma_1 b_2 Q}{(b_2Q+1)^2}+\gamma_0+\frac{\gamma_1}{b_2Q+1}\right)\lambda_5,\\
&= -\omega_2+\frac{\gamma_1}{1+b_2Q}\left(\frac{b_2Q}{1+b_2Q}-1\right)(\lambda_5-\lambda_4)+\gamma_0(\lambda_4-\lambda_5)+\mu\lambda_4,\\
\frac{d\lambda_5}{dt} &= -\frac{\partial H}{\partial R} = \mu\lambda_5,
\end{aligned}
$$

completed with the transversality condition $\lambda_i(t=T)=0$ for $i=1,2,3,4,5$. Furthermore, the optimal controls (u_1^*, u_2^*) are given by:

$$
\begin{aligned}
u_1^* &= \min\left\{\max\left\{u_1^{\min}, \frac{S\,(\lambda_1-\lambda_2)}{2\varphi_1}\right\}, u_1^{\max}\right\},\\
u_2^* &= \min\left\{\max\left\{u_2^{\min}, \frac{I\,(\lambda_3-\lambda_4)}{2\varphi_2}\right\}, u_2^{\max}\right\},
\end{aligned}
\tag{6.4}
$$

where $u_i^{\min}$ and $u_i^{\max}$, for $i=1,2$, represent the lower and upper bounds of u_1 and u_2, respectively.

6.2. Optimal control simulations

The solution of our optimal control problem in Eq (6.4) through analytical methods is unattainable due to the high dimensionality and nonlinearity of the ordinary differential equations system for the state variables in Model (2.1) and the adjoint variable in (6.3). Consequently, we employ a forward-backward sweep method to solve our problem numerically [73]. Additional examples demonstrating the implementation of this method can be found in [76–79]. The initial step involves providing an initial guess for the control variables u_1 and u_2 for all $t \in [0,T]$. By combining this guess with an initial condition for the state variables, we solve Model (2.1) in the time interval $t \in [0,T]$ forward in time. Subsequently, utilizing the obtained results, we solve the adjoint system in (6.3) backward in time, subject to the transversality condition $\lambda_i(T)=0$. With the solutions for the state and adjoint variables in hand, we update the control variables using the formula in (6.4). This iterative process is repeated until the convergence criteria is met, with convergence defined as $|J^{\text{iteration-k+1}} - J^{\text{iteration-k}}| \le 10^{-5}$.

We have divided the numerical experiments in this section into three different categories for three different purposes. The first simulation is conducted to determine the most cost-effective scenario based on the combination of controls. The second simulation aims to assess the impact of the initial population condition on the dynamics of control. The last simulation is conducted to evaluate the influence of the initial basic reproduction number on the effectiveness of the COVID-19 control strategy.

6.2.1. Simulation for different strategies

In this section, we conducted a numerical experiment to address our optimal control problem, exploring various combinations of control interventions. The first scenario involves the simultaneous implementation of vaccination and quarantine measures to contain the spread of COVID-19. The outcomes are presented in Figure 6. It is evident that when both of these interventions are employed concurrently, there is a notable reduction in the number of infected individuals. The dynamics of vaccination control necessitate an initial high rate of application during the early stages of the simulation,

followed by a gradual decrease over time. Conversely, the quarantine intervention exhibits a decreasing trend in response to a heightened number of infected individuals being placed under quarantine. The total cost of intervention for this scenario is 3.51×10^6.

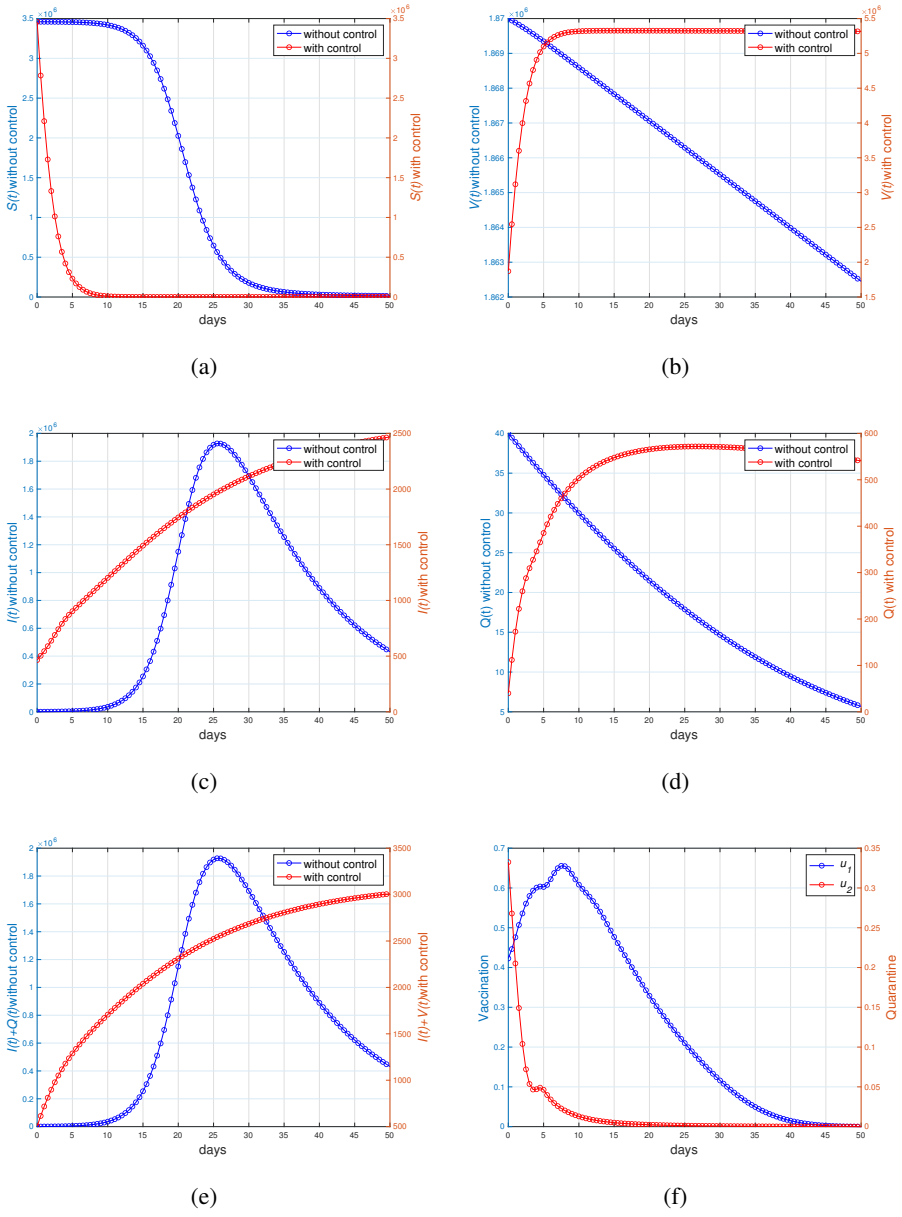

Figure 6. Optimal control results when vaccination and quarantine are implemented together. Panels (a)–(f) represent the dynamics of S, V, I, Q, $I + Q$ and control variables, respectively. The total infected averted with this scenario is 4.014×10^7, with a total cost for intervention of 3.47×10^6.

The subsequent simulation aims to elucidate the population's response when vaccination is implemented as the sole intervention. The results are presented in Figure 7. It is evident that without quarantine measures, vaccination intervention necessitates a more intensive application, as indicated in panel (f). Consequently,

the vaccinated population approaches nearly the entire total population, while the number of infected individuals, although exhibiting an increase, remains significantly lower in comparison to scenarios without any control measures. The overall cost of intervention in this scenario is only marginally higher than that of the first scenario, where vaccination and quarantine are implemented concurrently.

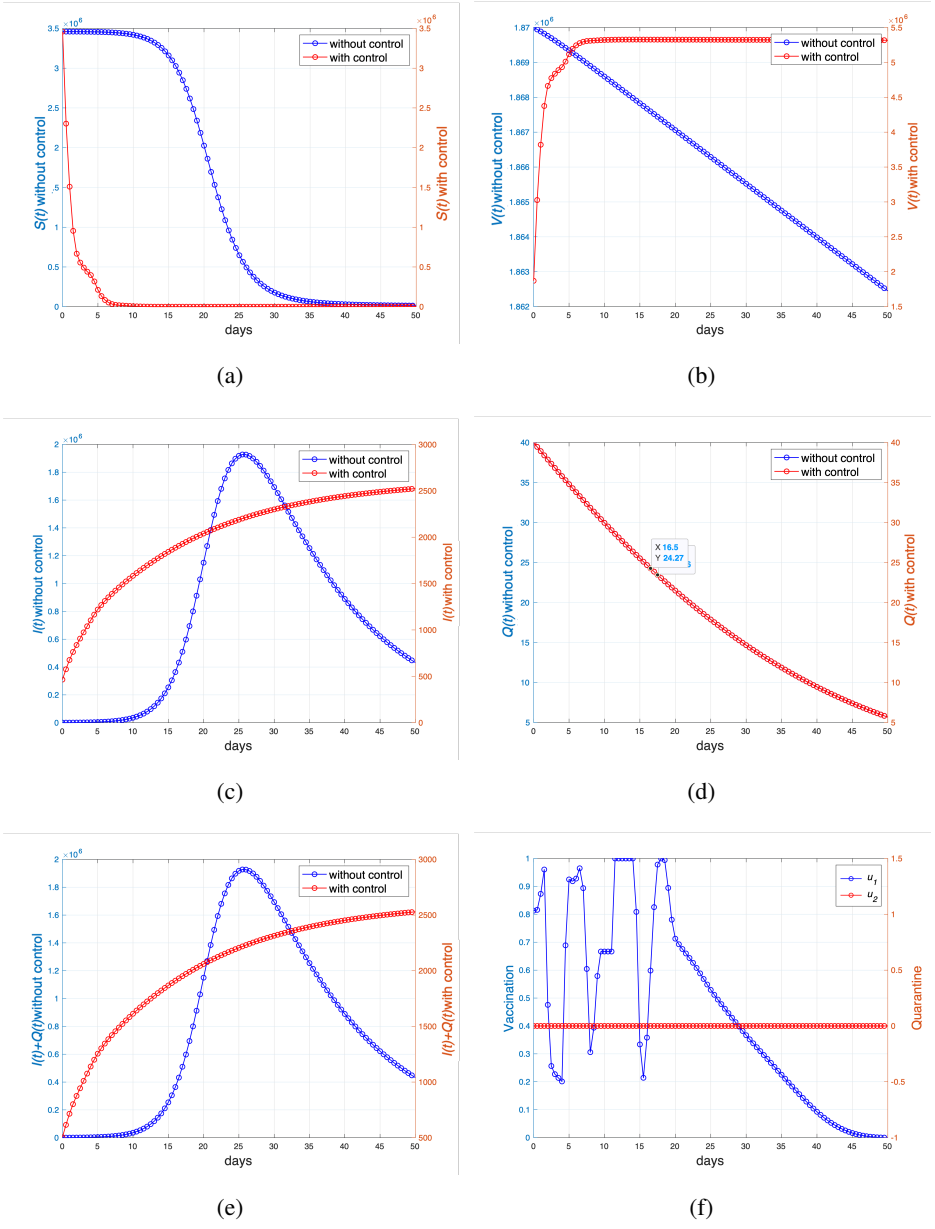

Figure 7. Optimal control results when vaccination and quarantine are implemented together. Panels (a)–(f) represent the dynamics of S, V, I, Q, $I + Q$ and control variables, respectively. The total infected averted with this scenario is 4.02×10^7, with a total cost for intervention of 3.51×10^6.

The final simulation was conducted to assess the impact of quarantine intervention when employed

as the sole measure to mitigate COVID-19. The results are depicted in Figure 8. It is evident that without vaccination intervention, quarantine measures do not have a significant effect on curtailing the number of infected individuals, unlike the two preceding scenarios. To counterbalance the high number of infections, intensive vaccination interventions must be administered in the initial stages (refer to panel (f)). However, since our model assumes that the recovery of quarantined individuals follows a saturation function, it becomes increasingly challenging to increase the recovery rate as more individuals are placed under quarantine. This is because there are a high number of individuals who require treatment. Therefore, this intervention must be scaled back over time to minimize intervention costs. Consequently, quarantine interventions do not yield significant results in reducing infection numbers, as observed in the two previous scenarios.

6.2.2. Simulation for different initial conditions

In contrast to the simulations in the previous subsection, which focused on intervention combinations, this subsection focuses on scenarios driven by distinct initial conditions. These simulations are conducted under the assumption of very low initial infection counts, and this scenario can be termed an endemic prevention scenario, where intervention is implemented before rapid COVID-19 transmission occurs. The initial condition is given by:

$$S(0) = 5\,330\,000, \quad V(0) = 0, \quad I(0) = 100, \quad Q(0) = 0, \quad R(0) = 0.$$

The simulation outcomes are illustrated in Figure 9. It is evident that when the number of infected individuals at the initial time is extremely low, the intervention administered is also relatively modest (refer to panel (f) in the blue curve). Vaccination intervention begins to escalate as the number of infected individuals increases (see panels (c)–(e) highlighted in red). On the other hand, the intensity of quarantine intervention diminishes over time, reflecting the reduced effectiveness of treatment intervention for individuals who are quarantined. This is due to the increasing number of individuals who are subject to quarantine. The total cost incurred for this scenario is 5.33×10^6, which is greater than when the initial condition involved a higher number of infected individuals. However, the number of new infections successfully averted is substantially larger, amounting to 6.51×10^7.

6.2.3. Simulation for different initial basic reproduction numbers

The final simulation in this chapter was conducted to assess the influence of the endemic level, as indicated by the magnitude of $\mathscr{R}_c$ in the population, on the intensity of control measures required to manage COVID-19. To achieve this, the parameters used were consistent with those in Table 1, except for β_1 and β_2, which were reduced by 50%. As a result, we obtained $\mathcal{R}_c = 4.658$, which is 50% smaller than the estimate from the previous chapter. The results are displayed in Figure 10. Due to the lower value of $\mathscr{R}_c$, the intensity of vaccination control shown in Figure 10 (panel (f)) does not need to be as high as indicated in Figure 6 (panel (f)). Nonetheless, interventions of this nature have proven effective in significantly reducing the number of infected individuals (see panel (e)). The total cost incurred in this scenario is 9.43×10^6, which is substantially smaller than the scenario in Figure 6. The number of infections successfully averted amounts to 3.4×10^6.

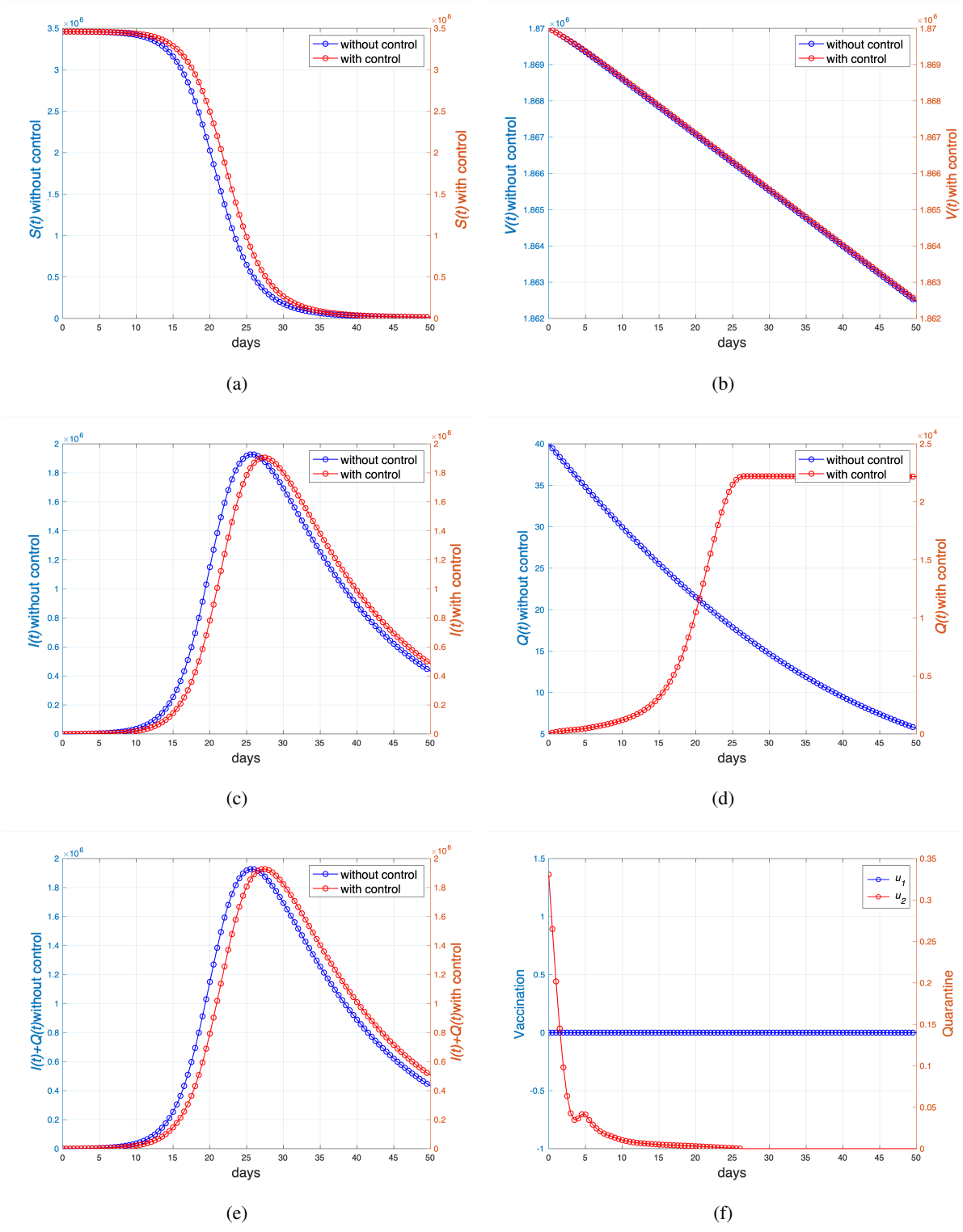

Figure 8. Optimal control results when vaccination and quarantine are implemented together. Panels (a)–(f) represent the dynamics of S, V, I, Q, $I + Q$ and control variables, respectively. The total infected averted with this scenario is 3.12×10^5, with a total cost for intervention of 3.51×10^6.

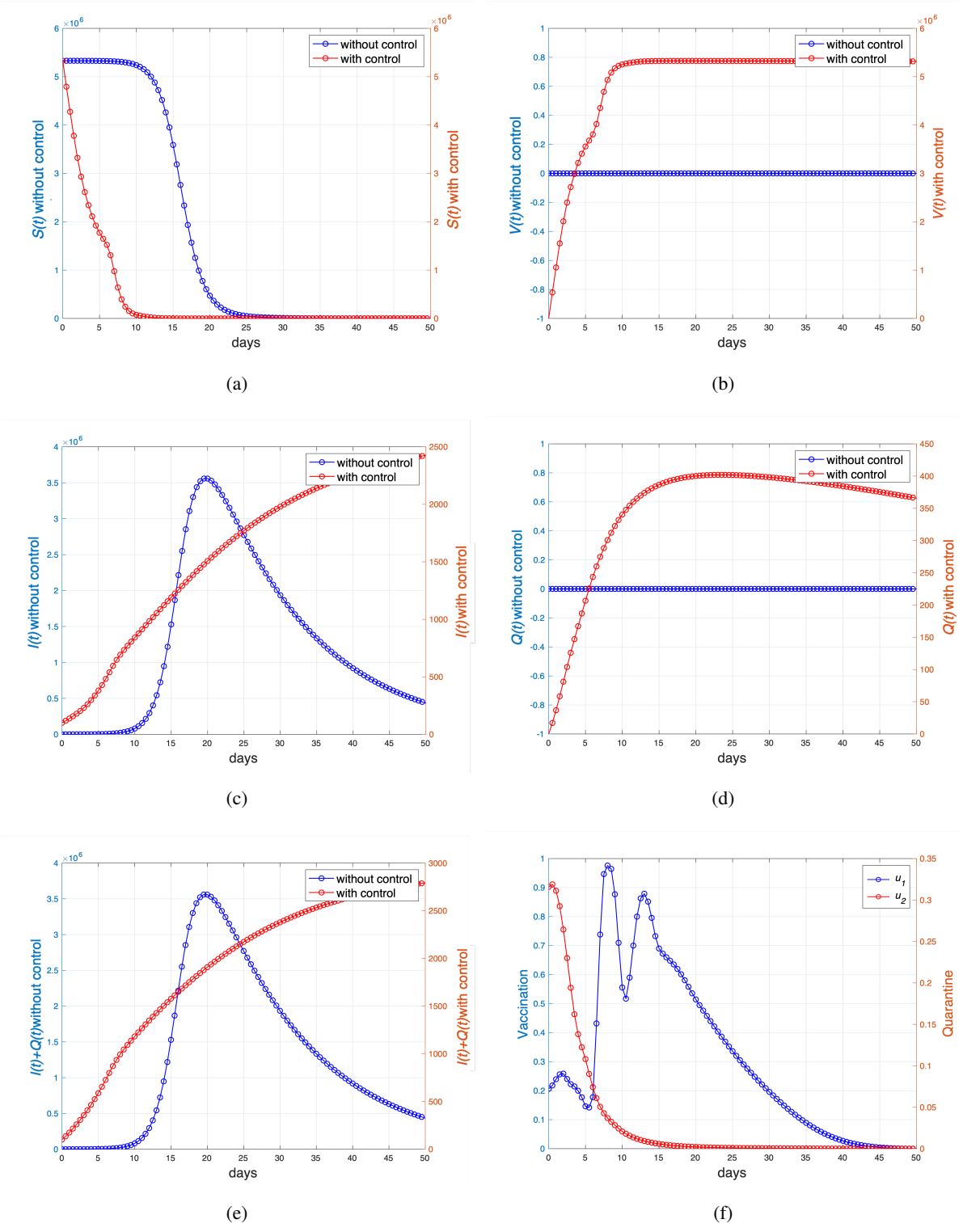

Figure 9. Optimal control results when vaccination and quarantine are implemented together but when COVID-19 has just started to spread (indicated by the small number of infected individuals at $t = 0$). Panels (a)–(f) represent the dynamics of S, V, I, Q, $I + Q$ and control variables, respectively. The total infected averted with this scenario is 6.51×10^7, with a total cost for intervention of 5.33×10^6.

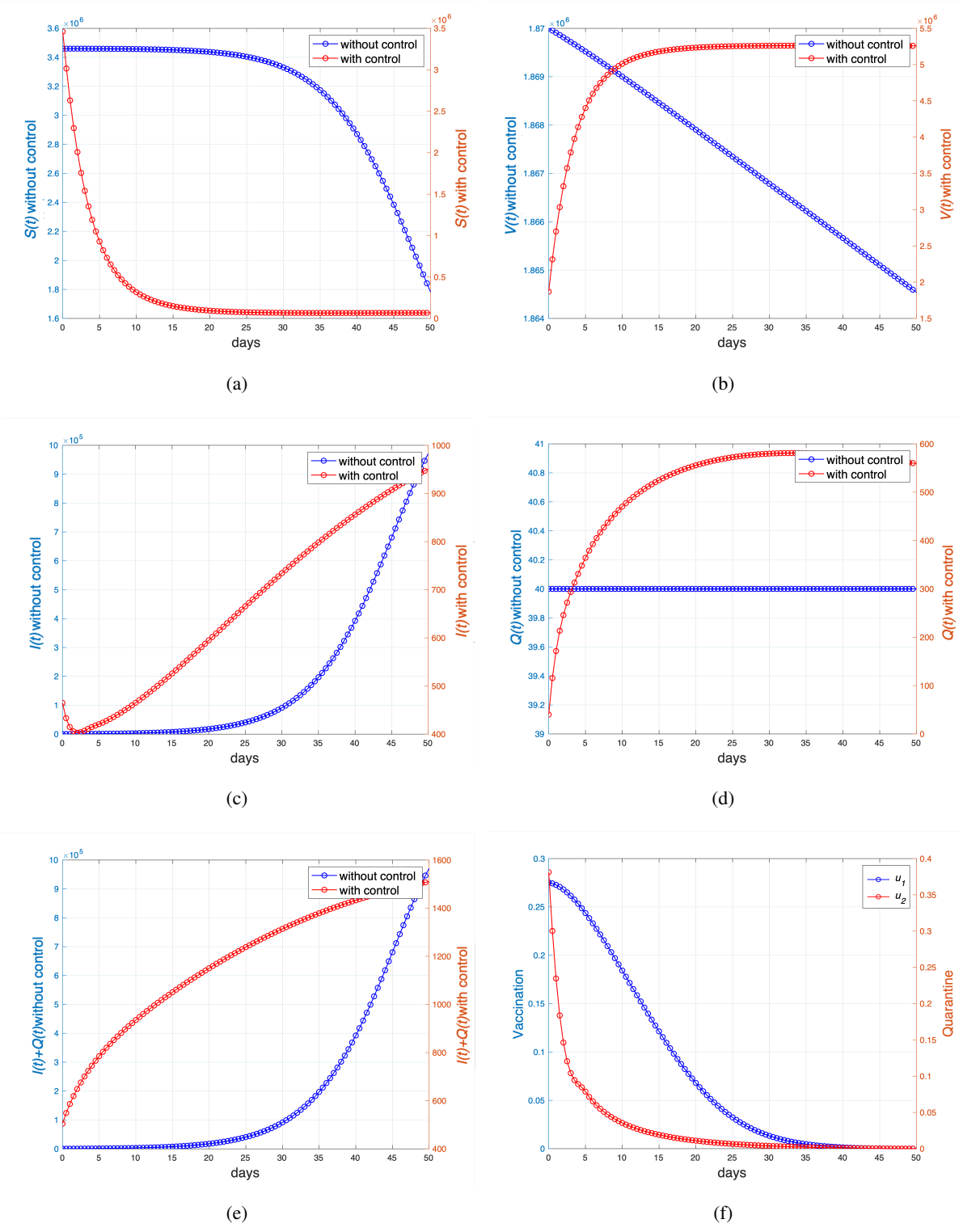

Figure 10. Optimal control results when the initial basic reproduction number is smaller, i.e., $\mathscr{R}_c = 4.658$, which is 50% smaller than in scenario one in Section 6.2.1. Panels (a)–(f) represent the dynamics of S, V, I, Q, $I + Q$ and control variables, respectively. The total infected averted with this scenario is 9.43×10^6, with a total cost for intervention of 3.4×10^6.

7. Discussion and conclusions

In this paper, we delved into an analysis of the dynamic characteristics of the COVID-19 transmission model, specifically the susceptible-vaccinated-infected-quarantine-recovered ($SVIQR$) model. Our investigation considers critical factors such as human awareness and resource constraints for treating quarantined individuals. To estimate model parameters, we utilized incidence data sourced from West Java, Indonesia. Our exploration encompassed mathematical analyses of equilibrium points, their local stability, and the control reproduction number ($\mathscr{R}_c$), all of which are presented analytically.

Our findings revealed a significant insight: The model may display forward or backward bifurcations at $\mathscr{R}_c = 1$. This suggests that achieving a reproductive number below one alone is not always sufficient to ensure the complete eradication of COVID-19 from a population. This result is consistent with another COVID-19 model introduced in [33, 76]. In practice, backward bifurcation commonly occurs due to several possible factors, such as reinfection [80], relapse, imperfect vaccination [81, 82], or limited treatment capacity [83]. In the context of our study on COVID-19, the existence of the backward bifurcation suggests the potential for decision-making challenges, as the expectation that COVID-19 will always disappear when $\mathscr{R}_c < 1$ is not consistently observed in real-world scenarios. The implications of this backward bifurcation highlight the possibility of a significant shift from a stable COVID-19-free state to a large endemic state, emphasizing the complex dynamics of disease control in public health. Another important result of our research is the sensitivity analysis. Sensitivity analysis underscores the potential effectiveness of minimizing contact between infected individuals who are not in quarantine and vaccinated individuals as a means of controlling the disease's spread.

To address budget limitations, we reconstructed our model as an optimal control model, introducing vaccination and quarantine interventions as time-dependent parameters. By employing Pontriagin's maximum principle, we rigorously formulated our optimal control problem and utilized the forward-backward sweep method for numerical solutions. Our simulations, conducted across various scenarios that may manifest in real-world situations, yielded noteworthy insights.

To begin, our numerical experiments underscore the paramount importance of vaccination as the primary intervention in curtailing infections. Vaccination has been proven effective in reducing the likelihood of vaccinated individuals contracting the virus, thereby minimizing the number of infected individuals. However, combining vaccination with quarantine measures still yields more promising results than relying solely on vaccination. A second critical finding emphasizes the necessity of implementing interventions at the onset of an outbreak rather than waiting for it to escalate. This early intervention strategy leads to a significantly higher number of preventable infections. The results of our optimal control simulation study underscore the importance of considering vaccination and quarantine strategies in controlling the spread of COVID-19. Both interventions play distinct roles: Vaccination is highly effective in preventing the initial spread of COVID-19 during the early stages of the pandemic, while quarantine measures are best focused as the pandemic begins to escalate. The combination of both strategies is essential for effectively mitigating the outbreak of COVID-19. Implementing these strategies based on needs will yield optimal results, resulting in a reduced budget for intervention and preventing a larger number of COVID-19 infections.

While our study sheds considerable light on the significance of the COVID-19 vaccination, there are several possible future directions in COVID-19 research from this article and other references from other disciplines. In many instances, there exists a gap between genetics, environmental science, and

epidemiology in the context of COVID-19. Potential novel insights lie in understanding the determinants of COVID-19 susceptibility and informing targeted interventions and public health strategies to mitigate the impact of the pandemic. Readers can explore a mathematical approach for this scenario in [84]. Another promising avenue in COVID-19 modeling involves bridging rumor spreading models with COVID-19 dynamics, leveraging insights from the Maki-Thompson model [85]. Readers can adapt the Maki-Thompson model to incorporate elements relevant to COVID-19 transmission dynamics, such as contact rates, transmission probabilities, and population demographics. Furthermore, readers can delve into research directions by exploring the concept of strategic decision-making and resource allocation in the context of pandemic response, utilizing a stochastic control approach [86]. Through this approach, we can gain a better understanding of the effectiveness of strategies for managing public health crises and ultimately contribute to improved preparedness and resilience in the face of future pandemics. In conclusion, by embracing interdisciplinary approaches and leveraging mathematical modeling techniques, we can pave the way for innovative solutions to combat COVID-19 and enhance our preparedness for future pandemics.

Use of AI tools declaration

The authors declare they have not used Artificial Intelligence (AI) tools in the creation of this article.

Acknowledgments

This research is funded by Universitas Indonesia through the PUTI Research Grant Scheme, 2023 (ID Number: NKB-469/UN2.RST/HKP.05.00/2023).

Conflict of interest

The authors declare there is no conflict of interest.

References

1. *The World Health Organization (WHO)*, Coronavirus disease (covid-19) pandemic, 2023. Available from: https://www.who.int/europe/emergencies/situations/covid-19.
2. *Centers for Disease Control and Prevention*, Symptoms of covid-19, 2023. Available from: https://www.cdc.gov/coronavirus/2019-ncov/symptoms-testing/symptoms.html.
3. *The World Health Organization (WHO)*, Indonesia situation of covid-19, 2023. Available from: https://covid19.who.int/region/searo/country/id.
4. *Ministry of State Apparatus Utilization and Bureaucratic Reform, Indonesia (KEMEN-PANRI)*, Indonesia telah bergerak menuju endemi covid-199, 2023. Available from: https://www.menpan.go.id/site/berita-terkini/berita-daerah/indonesia-telah-bergerak-menuju-endemi-covid-19.

5. *Communication Team of the National Committee for Handling Corona Virus Disease 2019 (Covid-19) and National Economic Recovery, Indonesia*, Waspadai komorbid, salah satu faktor risiko yang memperparah gejala covid-19, 2022. Available from: https://covid19.go.id/artikel/2022/02/15/waspadai-komorbid-salah-satu-faktor-risiko-yang-memperparah-gejala-covid-19.
6. *The Ministry of Health Republic Indonesia (KEMENKES RI)*, Covid 19 update, 2023. Available from: https://www.mayoclinic.org/diseases conditions/coronavirus/in-depth/herd-immunity-and coronavirus.
7. K. Cardwell, B. Clyne, N. Broderick, B. Tyner, G. Masukume, L. Larkin, et al., Lessons learnt from the covid-19 pandemic in selected countries to inform strengthening of public health systems: a qualitative study, *Public Health*, **225** (2023), 343–352. https://doi.org/10.1016/j.puhe.2023.10.024
8. F. M. Ekawati, M. Muchlis, N. G. Iturrieta-Guaita, D. A. D. Putri, Recommendations for improving maternal health services in indonesian primary care under the covid-19 pandemic: Results of a systematic review and appraisal of international guidelines, *Sex. Reprod. Healthcare*, **35** (2023), 100811. https://doi.org/10.1016/j.srhc.2023.100811
9. A. Rupp, P. Limpaphayom, Benefits of corporate social responsibility during a pandemic: Evidence from stock price reaction to covid-19 related news, *Res. Int. Bus. Finance*, **68** (2024), 102169. https://doi.org/10.1016/j.ribaf.2023.102169
10. I. D. Selvi, Online learning and child abuse: the covid-19 pandemic impact on work and school from home in indonesia, *Heliyon*, **8** (2022), e08790. https://doi.org/10.1016/j.heliyon.2022.e08790
11. R. Banerjee, R. K. Biswas, Fractional optimal control of compartmental sir model of covid-19: Showing the impact of effective vaccination, *IFAC-PapersOnLine*, **55** (2022), 616–622. https://doi.org/10.1016/j.ifacol.2022.04.101
12. M. L. Diagne, H. Rwezaura, S. Y. Tchoumis, J. M. Tchuenche, A mathematical model of covid-19 with vaccination and treatment, *Comput. Math. Methods Med.*, **2021** (2021), 1250129. https://doi.org/10.1155/2021/1250129
13. J. N. Paul, I. S. Mbalawata, S. S. Mirau, L. Masandawa, Mathematical modeling of vaccination as a control measure of stress to fight covid-19 infections, *Chaos, Solitons Fractals*, **166** (2023), 112920. https://doi.org/10.1016/j.chaos.2022.112920
14. B. Yang, Z. Yu, Y. Cai, The impact of vaccination on the spread of covid-19: Studying by a mathematical model, *Physica A*, **590** (2022), 126717. https://doi.org/10.1016/j.physa.2021.126717
15. A. Ayalew, M. Yezbalew, T. Tilahun, T. Tesfa, Mathematical model and analysis on the impacts of vaccination and treatment in the control of the covid-19 pandemic with optimal control, *J. Appl. Math.*, **2023** (2023), 8570311. https://doi.org/10.1155/2023/8570311
16. C. W. Chukwu, R. T. Alqahtani, F. F. Herdicho, A pontryagin's maximum principle and optimal control model with cost-effectiveness analysis of the covid-19 epidemic, *Decis. Anal. J.*, **8** (2023), 100273. https://doi.org/10.1016/j.dajour.2023.100273
17. S. Bhatter, K. Jangid, A. Abidemi, K. M. Owolabi, S. D. Purohit, A new fractional mathematical model to study the impact of vaccination on covid-19 outbreaks, *Decis. Anal. J.*, **6** (2023), 100156. https://doi.org/10.1016/j.dajour.2022.100156

18. C. Xu, Y. Yu, G. Ren, Y. Sun, X. Si, Stability analysis and optimal control of a fractional-order generalized seir model for the covid-19 pandemic, *Appl. Math. Comput.*, **457** (2023), 128210. https://doi.org/10.1016/j.amc.2023.128210

19. C. M. Wachira, G. O. Lawi, L. O. Omondi, Travelling wave analysis of a diffusive covid-19 model, *J. Appl. Math.*, **2022** (2022), 60522274. https://doi.org/10.1155/2022/6052274

20. B. Barnes, I. Takyi, B. E. Owusu, F. Ohene Boateng, A. Saahene, E. Saarah Baidoo, et al., Mathematical modelling of the spatial epidemiology of covid-19 with different diffusion coefficients, *Int. J. Differ. Equations*, **2022**, 7563111. https://doi.org/10.1155/2022/7563111

21. A. El Koufi, N. El Koufi, Stochastic differential equation model of covid-19: Case study of pakistan, *Results Phys.*, **34** (2022), 105218. https://doi.org/10.1016/j.rinp.2022.105218

22. M. Pajaro, N. M. Fajar, A. A. Alonso, I. Otero-Muras, Stochastic sir model predicts the evolution of covid-19 epidemics from public health and wastewater data in small and medium-sized municipalities: A one year study, *Chaos, Solitons Fractals*, **164** (2022), 112671. https://doi.org/10.1016/j.chaos.2022.112671

23. V. V. Khanna, K. Chadaga, N. Sampathila, R. Chadaga, A machine learning and explainable artificial intelligence triage-prediction system for covid-19, *Decis. Anal. J.*, **7** (2023), 100246. https://doi.org/10.1016/j.dajour.2023.100246

24. K. Moulaei, M. Shanbehzadeh, Z. Mohammadi-Taghiabad, H. Kazemi-Arpanahi, Comparing machine learning algorithms for predicting covid-19 mortality, *BMC Med. Inf. Decis. Making*, **22** (2022), 1–12. https://doi.org/10.1186/s12911-021-01742-0

25. D. Aldila, S. H. Khoshnaw, E. Safitri, Y. R. Anwar, A. R. Bakry, B. M. Samiadji, et al., A mathematical study on the spread of covid-19 considering social distancing and rapid assessment: the case of jakarta, indonesia, *Chaos Solitons Fractals*, **139** (2020), 110042. https://doi.org/10.1016/j.chaos.2020.110042

26. J. L. Gevertz, J. M. Greene, C. H. Sanchez-Tapia, E. D. Sontag, A novel covid-19 epidemiological model with explicit susceptible and asymptomatic isolation compartments reveals unexpected consequences of timing social distancing, *J. Theor. Biol.*, **510** (2021), 110539. https://doi.org/10.1016/j.jtbi.2020.110539

27. I. A. Arik, H. K. Sari, S. I. Araz, Numerical simulation of covid-19 model with integer and non-integer order: The effect of environment and social distancing, *Results Phys.*, **51** (2023), 106725. https://doi.org/10.1016/j.rinp.2023.106725

28. S. Saharan, C. Tee, A covid-19 vaccine effectiveness model using the susceptible-exposed-infectious-recovered model, *Healthcare Anal.*, **4** (2023), 100269. https://doi.org/10.1016/j.health.2023.10026

29. A. I. Alaje, M. O. Olayiwola, A fractional-order mathematical model for examining the spatiotemporal spread of covid-19 in the presence of vaccine distribution, *Healthcare Anal.*, **4** (2023), 100230. https://doi.org/10.1016/j.health.2023.100230

30. R. Pino, V. M. Mendoza, E. A. Enriques, A. C. Velasco, R. Mendoza, An optimization model with simulation for optimal regional allocation of covid-19 vaccines, *Healthcare Anal.*, **4** (2023), 100244. https://doi.org/10.1016/j.health.2023.100244

31. O. J. Watson, G. Barnsley, J. Toor, A. B. Hogan, P. Winskill, A. C. Ghani, Global impact of the first year of covid-19 vaccination: a mathematical modelling study, *Lancet Infect. Dis.*, **22** (2022), 1293–1302. https://doi.org/10.1016/S1473-3099(22)00320-6
32. A. K. Paul, M. A. Kuddus, Mathematical analysis of a covid-19 model with double dose vaccination in bangladesh, *Results Phys.*, **35** (2022), 105392. https://doi.org/10.1016/j.rinp.2022.105392
33. O. I. Idisi, T. T. Yusuf, K. M. Owolabi, B. A. Ojokoh, A bifurcation analysis and model of covid-19 transmission dynamics with post-vaccination infection impact, *Healthcare Anal.*, **3** (2023), 100157. https://doi.org/10.1016/j.health.2023.100157
34. I. Ul Haq, N. Ullah, N. Ali, K. S. Nisar, A new mathematical model of covid-19 with quarantine and vaccination, *Mathematics*, **11** (2022), 142. https://doi.org/10.3390/math11010142
35. D. S. A. A. Reza, M. N. Billah, S. S. Shanta, Effect of quarantine and vaccination in a pandemic situation: A mathematical modelling approach, *J. Math. Anal. Model.*, **2** (2021), 77–81. https://doi.org/10.48185/jmam.v2i3.318
36. Y. Gu, S. Ullah, M. A. Khan, Mathematical modeling and stability analysis of the covid-19 with quarantine and isolation, *Results Phys.*, **34** (2022), 105284. https://doi.org/10.1016/j.rinp.2022.105284
37. F. Wu, X. Liang, J. Lein, Modelling covid-19 epidemic with confirmed cases-driven contact tracing quarantine, *Infect. Dis. Modell.*, **8** (2023), 415–426. https://doi.org/10.1016/j.idm.2023.04.001
38. A. K. Saha, S. Saha, C. N. Podder, Effect of awareness, quarantine and vaccination as control strategies on covid-19 with co-morbidity and re-infection, *Infect. Dis. Modell.*, **7** (2022), 660–689. https://doi.org/10.1016/j.idm.2022.09.004
39. S. S. Musa, S. Queshi, S. Zhao, A. Yusuf, U. T. Mustapha, D. He, Mathematical modeling of covid-19 epidemic with effect of awareness programs, *Infect. Dis. Modell.*, **6** (2021), 448–460. https://doi.org/10.1016/j.idm.2021.01.012
40. A. A. Anteneh, Y. M. Bazazaw, S. Palanisam, Mathematical model and analysis on the impact of awareness campaign and asymptomatic human immigrants in the transmission of covid-19, *Biomed Res. Int.*, **2022** (2022), 6260262. https://doi.org/10.1155/2022/6260262
41. M. A. Balya, B. O. Dewi, F. I. Lestari, G. Ratu, H. Rosuliyana, T. Windyhani, et al., Investigating the impact of social awareness and rapid test on a covid-19 transmission model, *Commun. Biomathematical Sci.*, **4** (2021), 46–64. https://doi.org/10.5614/cbms.2021.4.1.5
42. A. K. Srivastav, M. Gosh, S. S. Bandekar, Modeling of covid-19 with limited public health resources: a comparative study of three most affected countries, *Eur. Phys. J. Plus*, **136** (2021), 359. https://doi.org/10.1140/epjp/s13360-021-01333-y
43. U. M. Rifanti, A. R. Dewi, N. Nurlaili, S. T. Hapsari, Model matematika covid-19 dengan sumber daya pengobatan yang terbatas, *J. Math. Appl.*, **18** (2021), 23–36. https://doi.org/10.12962/limits.v18i1.8207
44. S. Cakan, Dynamic analysis of a mathematical model with health care capacity for covid-19 pandemic, *Chaos, Solitons, Fractals*, **139** (2020), 110033. https://doi.org/10.1016/j.chaos.2020.110033
45. I. I. Oke, Y. T. Oyebo, O. F. Fakoya, V. S. Benson, Y. T. Tunde, A mathematical model for covid-19 disease transmission dynamics with impact of saturated treatment: Modeling, analysis and simulation, *Open Access Lib. J.*, **8** (2021), 1–20. https://doi.org/10.4236/oalib.1107332

46. M. Elhia, L. Boujallal, M. Alkama, O. Balatif, M. Rachik, Set-valued control approach applied to a covid-19 model with screening and saturated treatment function, *Complexity*, **2020** (2020), 9501028. https://doi.org/10.1155/2020/9501028

47. J. K. Ghosh, S. K. Bhiswas, S. Sarkar, U. Ghosh, Mathematical modelling of covid-19: A case study of italy, *Math. Comput. Simul.*, **194** (2022), 1–18. https://doi.org/10.1016/j.matcom.2021.11.008

48. R. T. Alqahtani, A. Ajbar, Study of dynamics of a covid-19 model for saudi arabia with vaccination rate, saturated treatment function and saturated incidence rate, *Mathematics*, **9** (2021), 3134. https://doi.org/10.3390/math9233134

49. I. Ali, S. U. Khan, Dynamics and simulations of stochastic covid 19 epidemic model using legendre spectral collocation method, *AIMS Math.*, **8** (2023), 4220–4236. https://doi.org/10.3934/math.2023210

50. S. S. Chaharborj, S. S. Chaharborj, J. H. Asl, P. S. Phang, Controlling pandemic covid-19 using optimal control theory, *Results Phys.*, **26** (2021), 104311. https://doi.org/10.1016/j.rinp.2021.104311

51. R. P. Kumar, S. Basu, P. K. Santra, D. Ghosh, G. S. Mahapatra, Optimal control design incorporating vaccination and treatment on six compartment pandemic dynamical system, *Results Control Optim.*, **7** (2022), 100115. https://doi.org/10.1016/j.rico.2022.100115

52. T. Li, Y. Guo, Optimal control and cost-effectiveness analysis of a new covid-19 model for omicron strain, *Physica A*, **606** (2022), 128134. https://doi.org/10.1016/j.physa.2022.128134

53. A. Bilgram, P. G. Jensen, K. Y. Jørgensen, K. G. Larsen, M. Mikučionis, M. Muñiz, et al., An investigation of safe and near-optimal strategies for prevention of covid-19 exposure using stochastic hybrid models and machine learning, *Decis. Anal. J.*, **5** (2022), 100141. https://doi.org/10.1016/j.dajour.2022.100141

54. M. S. Khatun, S. Das, P. Das, Dynamics and control of an sitr covid-19 model with awareness and hospital bed dependency, *Chaos, Solitons Fractals*, **175** (2023), 114010. https://doi.org/10.1016/j.chaos.2023.114010

55. *Mayo Clinic*, Herd immunity and covid-19: What you need to know, 2023. Available from: https://www.mayoclinic.org/diseases conditions/coronavirus/in-depth/herd-immunity-and coronavirus.

56. D. K. A. Mannan, K. M. Farhana, Knowledge, attitude and acceptance of a covid-19 vaccine: a global cross-sectional study, *Int. Res. J. Bus. Social Sci.*, **6** (2020), 1–23.

57. S. M. Saeied, M. M. Saeied, I. A. Kabbash, S. Abdo, Vaccine hesitancy: beliefs and barriers associated with covid-19 vaccination among egyptian medical students, *J. Med. Virol.*, **93** (2021), 4280–4291. https://doi.org/10.1002/jmv.26910

58. M. O. Elgendy, M. E. A. Abdelrahim, Public awareness about coronavirus vaccine, vaccine acceptance, and hesitancy, *J. Med. Virol.*, **93**.(2021), 6535–6543. https://doi.org/10.1002/jmv.27199

59. S. Funk, E. Gilad, C. Watkins, V. A. A. Jansen, The spread of awareness and its impact on epidemic outbreaks, *Proc. Natl. Acad. Sci.*, **106** (2009), 6872–6877. https://doi.org/10.1073/pnas.0810762106

60. G. Kelly, S. Petti, N. Noah, Covid-19, non-covid-19 and excess mortality rates not comparable across countries, *Epidemiol. Infect.*, **149** (2021), e176. https://doi.org/10.1017/S0950268821001850

61. S. Nourazari, S. R. Davis, R. Granovsky, R. Austin, D. J. Straff, J. W. Joseph, L. D. Sanchez, Decreased hospital admissions through emergency departments during the covid-19 pandemic, *Am. J. Emerg. Med.*, **42** (2021), 203–210. https://doi.org/10.1016/j.ajem.2020.11.029
62. *Statistics Center of West Java Province (BPS)*, Jumlah penduduk menurut kabupaten/kota (jiwa), 2018-2020, 2023. Available from: https://jabar.bps.go.id/indicator/12/133/1/jumlah-penduduk-menurut-kabupaten-kota.html.
63. A. Abidemi, J. O. Akanni, O. D. Makinde, A non-linear mathematical model for analysing the impact of covid-19 disease on higher education in developing countries, *Healthcare Anal.*, **3** (2023), 100193. https://doi.org/10.1016/j.health.2023.100193
64. E. A. Iboi, O. Sharomi, C. N. Ngonghala, A. B. Gumel, Mathematical modeling and analysis of covid-19 pandemic in nigeria, *Math. Biosci. Eng.*, **17** (2020), 7192–7220. https://doi.org/10.3934/mbe.2020369
65. *Statistics Center of West Java Province (BPS)*, [komponen ipg] usia harapan hidup 2020-2022, 2023. Available from: https://jabar.bps.go.id/indicator/40/185/1/-komponen-ipg-usia-harapan-hidup-.html.
66. S. Olaniyi, O. S. Obabiyi, K. O. Okosun, A. T. Oladipo, S. O. Adewale, Athematical modelling and optimal cost-effective control of covid-19 transmission dynamics, *Eur. Phys. J. Plus*, **135** (2021), 1–20. https://doi.org/10.1140/epjp/s13360-020-00954-z
67. A. Abate, A. Tiwari, S. Sastrys, Box invariance in biologically-inspired dynamical systems, *Automatica*, **45** (2009), 1601–1610. https://doi.org/10.1016/j.automatica.2009.02.028
68. P. Taylan, G. W. Weber, L. Liu, F. Yerlika-Ozkurt, On the foundations of parameter estimation for generalized partial linear models with b-splines and continuous optimization, *Comput. Math. Appl.*, **60** (2010), 134–143. https://doi.org/10.1016/j.camwa.2010.04.040
69. A. A. Tappe, M. Schulze, R. Schenkendorf, Neural odes and differential flatness for total least squares parameter estimation, *IFAC-PapersOnLine*, **55** (2020), 421–426. https://doi.org/10.1016/j.ifacol.2022.09.131
70. O. Aydogmuz, T. Ali Hakan, A modified multiple shooting algorithm for parameter estimation in odes using adjoint sensitivity analysis, *Appl. Math. Comput.*, **390** (2021), 125644. https://doi.org/10.1016/j.amc.2020.125644
71. S. Khalilpourazari, H. Hashemi Doulabi, A. O. Ciftcioglu, G. W. Weber, Gradient-based grey wolf optimizer with gaussian walk: Application in modelling and prediction of the covid-19 pandemic, *Expert Syst. Appl.*, **177** (2021), 114920. https://doi.org/10.1016/j.eswa.2021.114920
72. P. Driesche, J. Watmough, Reproduction numbers and sub-threshold endemic equilibria for compartmental models of disease transmissions, *Math. Biosci.*, **180** (2002), 29–48. https://doi.org/10.1016/S0025-5564(02)00108-6
73. M. Martcheva, *An Introduction to Mathematical Epidemiology*, Springer, Berlin, Germany, 2015.
74. C. Castillo–Chavez, B. Song, Dynamical models of tuberculosis and their applications, *Math. Biosci. Eng.*, **1** (2024), 361–404. https://doi.org/10.3934/mbe.2004.1.361
75. S. Leinhart, J. T. Workman, *Optimal Control Applied to Biological Models*, Taylor & Francis Group, CRC press, Boca Raton, Florida, USA, 2007.

76. D. Aldila, Cost-effectiveness and backward bifurcation analysis on covid-19 transmission model considering direct and indirect transmission, *Commun. Math. Biol. Neurosci.*, **2020** (2020), 49. https://doi.org/10.28919/cmbn/4779
77. D. Aldila, A. Nadya, Fatmawati, F. F. Herdicho, M. Z. Ndii, C. W. Chukwu, Optimal control of pneumonia transmission model with seasonal factor: Learning from jakarta incidence data, *Heliyon*, **9** (2023), e18096. https://doi.org/10.1016/j.heliyon.2023.e18096
78. D. Aldila, M. Angelina, Optimal control problem and backward bifurcation on malaria transmission with vector bias, *Heliyon*, **7** (2021), e06824. https://doi.org/10.1016/j.heliyon.2021.e06824
79. D. Aldila, Optimal control for dengue eradication program under the media awareness effect, *Int. J. Nonlinear Sci. Numer. Simul.*, **24** (2023), 95–122. https://doi.org/10.1515/ijnsns-2020-0142
80. O. Sharomi, C. N. Podder, A. B, Gumel, B. Song, Mathematical analysis of the transmission dynamics of hiv/tb co-infection in the presence of treatment, *Math. Biosci. Eng.*, **5** (2008), 145–174. https://doi.org/10.3934/mbe.2008.5.145
81. E. H. Elbasha, C. N. Podder, A. B. Gumel, Analyzing the dynamics of an sirs vaccination model with waning natural and vaccine-induced immunity, *Nonlinear Anal. Real World Appl.*, **12** (2011), 2692–2705. https://doi.org/10.1016/j.nonrwa.2011.03.015
82. A. B. Gumel, Causes of backward bifurcations in some epidemiological models, *J. Math. Anal. Appl.*, **395** (2012), 355–365. https://doi.org/10.1016/j.jmaa.2012.04.077
83. D. Aldila, J. P. Chavez, K. P. Wijaya, N. C. Ganegoda, G. M. Simorangkir, H. Tasman, et al., A tuberculosis epidemic model as a proxy for the assessment of the novel m72/as01e vaccine, *Commun. Nonlinear Sci. Numer. Simul.*, **120** (2023), 107162. https://doi.org/10.1016/j.cnsns.2023.107162
84. K. Erik, W. Gerhard-Wilhelm, T. E. Babaee, Foundations of semialgebraic gene-environment networks, *J. Dyn. Games*, **7** (2020), 253–268. https://doi.org/10.3934/jdg.2020018
85. S. Belen, E. Kropat, W. Gerhard-Wilhelm, On the classical maki–thompson rumour model in continuous time, *Cent. Eur. Oper. Res.*, **19** (2011), 1–17. https://doi.org/10.1016/j.jmaa.2015.06.054
86. E. Savku, A stochastic control approach for constrained stochastic differential games with jumps and regimes, preprint, arXiv:2301.12921. https://doi.org/10.48550/arXiv.2301.12921

AIMS Press